Noble gases in the Cameroon line and the He, Ne, and Ar isotopic compositions of high mu (HIMU) mantle

JOURNAL OF GEOPHYSICAL RESEARCH, VOL. 104, NO. 12, PAGES 29,509–29,527, DECEMBER 10, 1999

Noble gases in the Cameroon line and the He, Ne, and Ar isotopic compositions of high μ (HIMU) mantle

Dan N. Barfod,[1,2] Chris J. Ballentine,[3] Alex N. Halliday,[1,3] and J. Godfrey Fitton[4]

Abstract. Ultramafic xenoliths, basaltic lavas, and CO_2 gases from the Cameroon line volcanic chain provide the first characterization of combined He, Ne, and Ar isotopes in a high-time-integrated $^{238}U/^{204}Pb = \mu$ (HIMU) magmatic system. Helium isotopic compositions typically range from 5.0 to $6.7R_a$, with an average of 6.3. These values are indistinguishable from the $^3He/^4He$ of other HIMU locales (Austral Islands, St. Helena). Neon isotopic compositions for xenoliths and CO_2 gases are mid-ocean ridge basalt (MORB)-like, with a maximum $^{20}Ne/^{22}Ne$ of 11.87 and $^{21}Ne/^{22}Ne$ of 0.0508. Argon isotopic compositions in silicates range from atmospheric to $^{40}Ar/^{36}Ar = 4910 \pm 430$ (crushing) and up to 16,300 ± 1000 (single grain, laser step heating). The correlation between $^{20}Ne/^{22}Ne$ and $^{40}Ar/^{36}Ar$ in CO_2 gases suggests a minimum $^{40}Ar/^{36}Ar = 1650 \pm 30$ for the mantle-derived component. Uniform $^3He/^4He$ in silicates and in CO_2 fluids across both the continental and oceanic sectors of the Cameroon line argues strongly for a negligible lithospheric contribution to noble gas isotopic compositions. This inference is supported by high $^{238}U/^3He$ in lherzolites, indicating that noble gases in these samples must have been recently introduced (<50,000 years ago) to the sample, most likely from the host magma. Ocean crust recycling models of mixing between MORB source regions and highly radiogenic slabs cannot produce the observed He and Ne isotopic compositions. Isolation and aging of MORB source mantle can generate the isotopic compositions but require extreme $^3He/^{22}Ne$ fractionation. Involvement of plume-derived gases, consistent with the lithophile element isotopic compositions, alleviates the need for strong $^3He/^{22}Ne$ fractionation. Closed-system aging of plume-derived heterogeneities can reproduce the data with minimum $^3He/^{22}Ne$ fractionation at reasonable $^{238}U/^3He$ ratios. However, diffusive exchange of He and to a lesser extent Ne between aged MORB source and aged plume veins could explain the occurrence of low $^3He/^4He$ compositions in all HIMU centers and the apparent low time-integrated $^3He/^{22}Ne$ of the Cameroon line.

1. Introduction

The majority of terrestrial volcanism is the direct result of plate tectonic processes, with the notable exception of intraplate volcanism. Isotopic heterogeneity among ocean island basalts (OIB) results from the isolation of source reservoirs having distinct time-integrated chemical compositions. These requirements have led to the development of several models for generating these reservoirs including delamination of continental lithosphere, metasomatism of the upper mantle, and melting of a primitive mantle or "predominant" mantle. The most widely accepted model is recycling and storage of oceanic crust and sediments which can account for much of the observed isotopic heterogeneity [*Hofmann*, 1997]. This simple and elegant model was first suggested by *Ringwood* [1975, 1990], and later expanded and modified by *Chase* [1981] and *Hofmann and White* [1982].

To account for the range of enriched and depleted OIB isotopic compositions, development of the oceanic plate recycling model has led to the identification of potential intermediate processes that modify the bulk chemistry of recycled lithosphere [*Hart and Staudigel*, 1989; *Ben Othman et al.*, 1989; *Weaver*, 1991]. These include (1) near-surface and subduction-related chemical fractionation such as increases in U/Pb and high field strength element enrichments, (2) the involvement of sedimentary and seawater components to account for high $^{207}Pb/^{204}Pb$ or $^{87}Sr/^{86}Sr$ [*Dupré and Allègre*, 1983], and (3) mixing processes within the mantle (e.g., homogenization of extreme compositions by mixing with mid-ocean ridge basalt (MORB) source mantle). The development of isotopic heterogeneities by in situ decay in the mantle requires considerable storage times. Time constraints are provided primarily by $^{207}Pb/^{204}Pb$–$^{206}Pb/^{204}Pb$ arrays for the MORB and OIB reservoirs [*Chase*, 1981], requiring 1–2 Gyr [*Hofmann*, 1997].

Ocean island basalts with very radiogenic Pb (resulting from high time-integrated $^{238}U/^{204}Pb = \mu$, termed HIMU) are thought to best represent the isotopic composition of recycled oceanic lithosphere, without the added signals from recycled sediments and only variable additions of MORB source mantle Pb [*Weaver*, 1991; *Chauvel et al.*, 1992]. Understanding the processes responsible for this mantle composition provides crucial insight into the evolution of the mantle system and the

[1]Department of Geological Sciences, University of Michigan, Ann Arbor.
[2]Now at Isotope Geosciences Unit, Scottish Universities Research and Reactor Center, East Kilbride, United Kingdom.
[3]Institute for Isotope Geology and Mineral Resources, Department of Earth Sciences, ETH Zürich, Switzerland.
[4]Grant Institute of Geology, University of Edinburgh, Edinburgh, Scotland, United Kingdom.

Paper number 1999JB900280.
0148-0227/99/1999JB900280$09.00

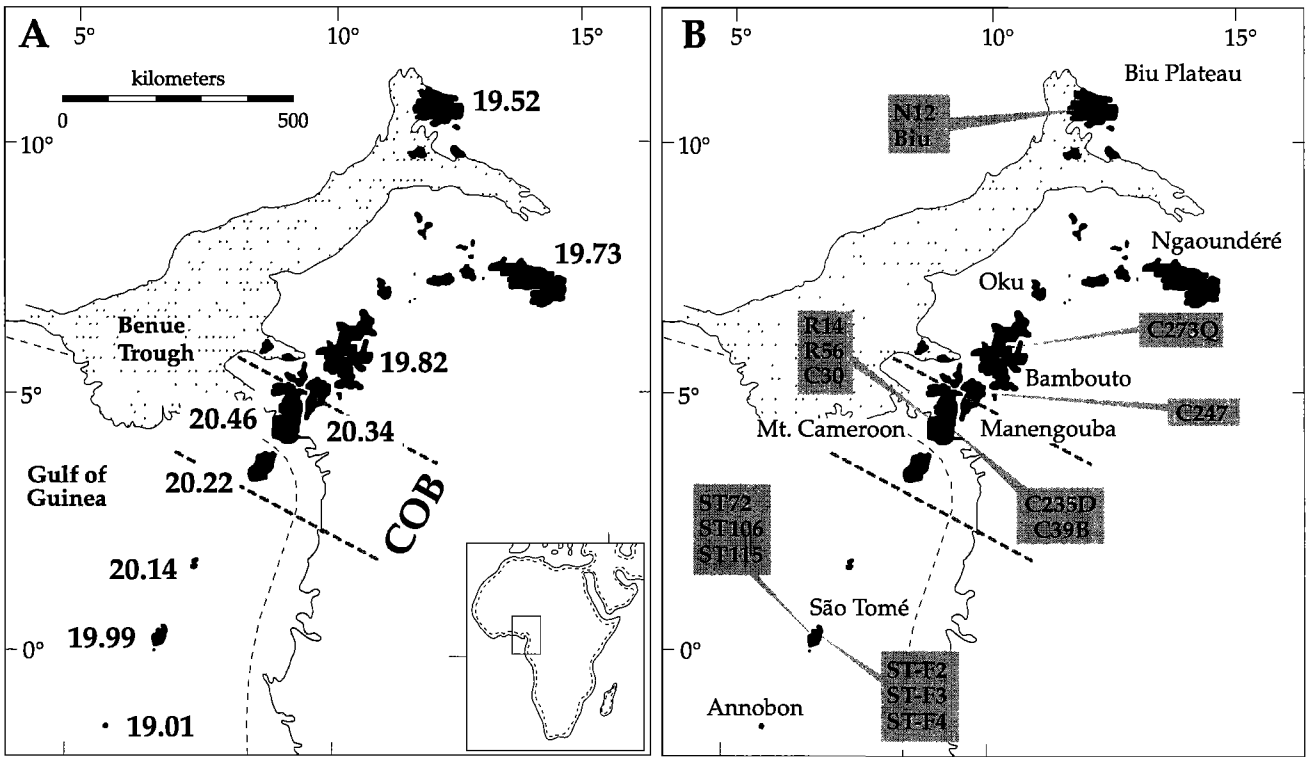

Figure 1. (a) The Cameroon line volcanic chain located in the Gulf of Guinea and West Africa (Nigeria and Cameroon). Volcanic centers are indicated as solid areas. Superimposed on the distribution of volcanic centers are $^{206}Pb/^{204}Pb$ data [*Halliday et al.*, 1988, 1990] for young volcanic rocks showing a pattern of increasingly radiogenic Pb toward the center of the chain at the continental crust-oceanic crust boundary (COB). (b) Xenolith samples restricted to the continental sector. Basaltic samples (all young and relatively undifferentiated) were obtained from the Mount Cameroon and Manengouba centers (R14, C30, C247), along with samples from São Tomé (ST-72, ST-106, ST-115). Carbon dioxide samples (ST-F series) were exclusively obtained from São Tomé, although the He isotopic data for the São Tomé fluids are very similar to the upper limit obtained in fluids from the continental sector, e.g., Lake Nyos R/R_a = 5.91 [*Sano et al.*, 1990].

fate of recycled oceanic crust. Classic HIMU basalts, such as those from St. Helena and Tubuaii, are also characterized by distinct and nearly uniform isotopic compositions of Hf and Nd [*Chauvel et al.*, 1992; *Hart et al.*, 1986; *Ballentine et al.*, 1997].

Treatment of noble gas systematics is conspicuously absent from recycling models, despite a considerable database for oceanic islands and MORB. As the oceanic crust is strongly degassed of primitive volatiles upon formation, by hydrothermal alteration near the surface, and by dehydration during subduction, it should possess a highly fractionated set of parent/daughter ratios (U + Th/He, U + Th/Ne, K/Ar). In a simple closed system, recycled oceanic crust should therefore rapidly acquire noble gas isotopic compositions that are highly radiogenic rather than retain primitive (MORB-like, R_a = 8 ± 1) compositions [*Hart*, 1984a; *Farley*, 1995]. In no case has any mantle sample produced isotopic compositions equivalent to the estimated mantle production ratios of He (R/R_a ~ 0.01–0.02) and Ne ($^{21}Ne/^{22}Ne$ ~ 0.4 to 32, see below).

In spite of these predictions the He isotopic compositions of HIMU OIB are generally slightly more radiogenic than those of MORB. Indeed, there is growing evidence that the isotopic composition of He in HIMU (5–7 R_a) is a robust indicator of source region composition [*Graham et al.*, 1992; *Hanyu and Kaneoka*, 1997; *Eiler et al.*, 1997; this study]. However, it has also been proposed that the lithosphere through which the magmas pass may provide radiogenic He [*Zindler and Hart*, 1986; *Hilton et al.*, 1995]. In this respect, it is essential to also identify the role of the lithosphere in controlling the observed noble gas isotopic compositions. Straddling both oceanic and continental lithosphere, the volcanic province of the Cameroon line is the ideal setting to evaluate the effects of migration through the lithosphere on the noble gas composition of HIMU magmas. We present results of the first combined He-Ne-Ar isotopic study of a HIMU system using the Cameroon line as a study area.

2. Geologic Setting and Sample Selection

The Cameroon line is an intraplate, alkaline volcanic province extending 1600 km from the African continental interior into the Gulf of Guinea to the island of Annobon (formerly Pagalu) (Figure 1). Mafic volcanic rocks are dominated by basanites and nephelinites with lesser hypersthene-normative basalts. Trace element patterns of mafic rocks (≥4.0 wt % MgO) are identical in both the continental and oceanic sectors of the volcanic chain, implying that lavas were generated below the lithospheric and were not obviously modified during ascent through the lithosphere [*Fitton*, 1987; *Fitton and Dunlop*, 1987].

Combined Pb, Sr, Nd, and Hf isotopic studies show striking temporal and spatial patterns within the mafic rocks of the Cameroon line. At the continent-ocean boundary (COB)

young (<10 Ma) lavas have radiogenic Pb ($^{206}Pb/^{204}Pb$ ~20.5) and unradiogenic Nd (ε_{Nd} +3), (Figure 1a) but with distance from the COB have less radiogenic Pb ($^{206}Pb/^{204}Pb$ ~ 19.0) and more radiogenic Ne (ε_{Nd} ~6) (Figure 1a) [*Halliday et al.*, 1988, 1990]. Lavas from Mount Cameroon and the ocean islands show systematic temporal progressions to more radiogenic Pb and Sr and less radiogenic Nd with decreasing age [*Halliday et al.*, 1988; *Lee et al.*, 1994]. In contrast to the Pb, Sr, and Nd isotopic trends the lavas of the oceanic Cameroon line have uniform Hf isotopic compositions. Hafnium isotopic compositions in the continental sector show more variation but have an average value (~+1.9ε_{Hf}) identical to that of the oceanic basalts [*Ballentine et al.*, 1997]. Although the Cameroon line does not possess Pb as radiogenic as that of the classic HIMU localities ($^{206}Pb/^{204}Pb$ up to 21.7), it does possess Hf and Nd isotopic compositions that are indistinguishable from those of other HIMU OIB [*White and Hofmann*, 1982; *Vidal et al.*, 1984; *Hart et al.*, 1986; *Nakamura and Tatsumoto*, 1988; *Weaver*, 1991; *Chauvel et al.*, 1992; *Ballentine et al.*, 1997].

Magmatic activity spans at least the past 65 Myr to the present, with several eruptions of Mount Cameroon in this century [*Fitton*, 1987]. Volcanic activity shows no systematic migration with time as expected for plume track migration, typified by the Hawaiian and Yellowstone systems. Instead, volcanic centers along the entire length of the chain have recently been active [*Fitton and Dunlop*, 1985]. However, initiation of volcanism in the ocean islands shows a pattern of outward progression, where basaltic rocks in the basal portions of each subaerial stratigraphic sequence become younger with distance from the COB, e.g., Príncipe, 31 Ma; São Tomé, 13 Ma; and Annobon, 4.8 Ma [*Lee et al.*, 1994]. *Lee et al.* [1994] interpret this feature as the outward propagation and lengthening of a sublithospheric "hot zone."

3. Analytical Procedures

Both xenolith and lava samples were coarsely crushed and sieved to 300 to 850 μm and then passed through a Frantz-Isodynamic magnetic separator. The minerals were ultrasonically cleaned for 30 min in 3.0 *N* HCl followed by 30 min in deionized H_2O to remove basalt adhering to crystal surfaces. Finally, samples were hand picked in ethanol under a binocular microscope using oblique illumination. In the early stages of this study, noble gases were extracted from mineral phases using an off-line crushing device. The device utilized two 1-cm stainless steel ball bearings placed within a 7-cm steel tube sealed with a 1-inch conflat cap (copper gasket). The crusher is shaken at ~15 strokes per second. An on-line technique was later developed based on a design similar to that of the earlier crushing device. Sequential crushing steps on gas rich olivine (R56, run C) using the on-line device showed ~95% gas release within the first minute and >99% within 3 min. All crushing steps (up to three 1-min steps) yielded identical He isotopic ratios within error, and we thus conclude that gases released by crushing are derived from fluid and/or melt inclusions within the samples [*Kurz*, 1986]. A third crushing technique was employed in the final part of the study, using an on-line solenoid driven crusher based on the design of *Kurz et al.* [1987].

Helium, neon, and argon were measured on the same sample splits. Noble gases were purified on an all-metal extraction system connected to two mass spectrometers. Argon was trapped on activated charcoal at liquid nitrogen temperatures. Helium and neon were trapped on a cryogenic pump at 12 K and 33 K, respectively. Helium was measured on a VG MM3000, 90° sector, gas source mass spectrometer, with a combined Faraday (^4He) and Johnston-type electron multiplier (^3He) collector array. Each sample analysis was bracketed by two air standard analyses for purposes of normalization and mass discrimination. The isotopic ratios of helium air standards measured in the MM3000 are independent of system pressure. Neon and Ar were measured on a MAP 215, 90° sector gas source mass spectrometer (Baur-Signer source) utilizing a Faraday collector and an electron multiplier equipped with ion counting to improve the signal-to-noise ratio.

Corrections for spectral interference of CO_2^{++} and $^{40}Ar^{++}$ on Ne masses 22 and 20, respectively, were empirical. The charge state ratio CO_2^{++}/CO_2^{+} decreases a step function with decreasing sample pressure; at gas pressures of $<2.6 \times 10^{-11}$ torr ^{20}Ne the ratio of CO_2^{++}/CO_2^{+} decreased from 0.010 to 0.007. Similar changes in charge state ratios measured in a gas source mass spectrometer were noted by *Hohenberg* [1980]. Hohenberg attributed this effect to increased residence times of ions in the source ionization chamber resulting from increases in pressure within the system. Notably, the opposite effect (increases in the fraction of doubly charged species with decreasing total system pressure) was found by *Niedermann et al.* [1997], although they did not speculate on the mechanisms controlling the charge state ratio in their system. Given differences in parameters such as source geometry or source-magnet field shape, variability in double charging effects is to be expected in different systems. The $^{40}Ar^{++}/^{40}Ar^{+}$ ratio did not deviate from a value of 0.197. Carbon dioxide and Ar were maintained at constant low pressures during analysis by use of a sintered stainless steel trap at liquid nitrogen temperatures. Bracketing each data collection block, CO_2^{+} and $^{40}Ar^{+}$ were monitored to establish a baseline correction. The effect of the CO_2 correction factor is most pronounced for $^{20}Ne/^{22}Ne$; employment of the correction factor is most pronounced for $^{20}Ne/^{22}Ne$; employment of the correction factor typically led to a change of 5% or less in $^{20}Ne/^{22}Ne$ and $^{21}Ne/^{22}Ne$. The contribution of $H_2\,^{18}O^{+}$ to the ^{20}Ne peak is negligible.

Air standard ratios (1σ errors) are $^{20}Ne/^{22}Ne$ = 9.882 (+0.012/−0.024), $^{21}Ne/^{22}Ne$ = 0.02874 (+0.00010/−0.00008), and $^{40}Ar/^{36}Ar$ = 298.8 ± 2.8. All samples are tube blank corrected for He, Ne, and Ar. Tube blanks are $4 \pm 3 \times 10^{-13}$ cm^3 ^{20}Ne STP and $7 \pm 2 \times 10^{-13}$ cm^3 ^{40}Ar STP, with ratios of $^{20}Ne/^{22}Ne$ ~5.0, $^{21}Ne/^{22}Ne$ ~0.2, and $^{40}Ar/^{36}Ar$ ~12.5. Helium tube blanks are atmospheric in composition and have intensities of $\sim 1.3 \times 10^{-9}$ cm^3 ^4He STP. Air standard ratios for He are reproducible within 1σ on a daily to weekly basis.

Reported errors on isotopic ratios take into account blank intensity and ratio, analytical uncertainty of ratio, and reproducibility of air standard ratios and are quoted to 1σ. Full procedural blanks are consistently atmospheric in composition and have intensities of 1.3×10^{-9} cm^3 ^4He STP, 1.3×10^{-11} cm^3 ^{20}Ne STP, and 3.8×10^{-9} cm^3 ^{40}Ar STP. The He procedural blank is dominated by the tube blank; this is due to prior use of the MM3000 for large-volume gas samples including air standards. Analyses of samples ST72, ST106, and ST115 were performed at Woods Hole Oceanographic Institution by M. Kurz (see *Kurz et al.* [1996] for analytical details).

We have included He isotopic analyses of two standard materials, 2πD43 MORB (popping rock) and olivine from a dunite xenolith (Re 496) obtained from the island of Réunion (Table 1). Our He data reproduce published values to within

Table 1. He Data

Sample	Location	Lithology	Phase	Run	Step	Mass, g	[^{4}He], cm^3 STP/g	R/R_a	$\pm1\sigma$
Xenoliths									
Biu V	Biu Plateau	clinopyroxenite vein in sp. lherzolite	cpx	A	1	2.00	2.97E-07	6.31	0.02
					2		8.45E-08	5.53	0.03
			cpx	B	1	1.02	2.51E-07	6.31	0.20
					2		1.56E-07	6.54	0.03
R56	Mt. Cameroon	dunite (cumulate)	olv	A	1	1.00	5.73E-07	5.66	0.16
					2		1.59E-07	5.21	0.02
			olv	B	1	2.10	1.46E-07	3.96	0.05
					2		1.39E-08	3.90	0.05
			olv	C	1	0.58	1.15E-06	5.15	0.15
					2		4.31E-08	5.29	0.20
					3		2.04E-08	5.26	0.24
C235D	Mt. Cameroon	lherzolite	olv			3.45	3.00E-09	5.54	0.21
			opx			1.53	1.00E-08	5.60	0.15
			cpx	A		1.29	2.51E-08	6.07	0.38
			cpx	B		3.00	8.31E-09	5.45	0.40
N12	Biu Plateau	harzburgite	olv	A		2.00	5.55E-09	5.01	0.30
			olv	B		3.37	7.04E-09	5.77	0.11
			olv	C		3.47	1.51E-08	5.80	0.06
			opx	A		1.00	8.66E-08	6.77	0.05
			opx	B		1.80	1.25E-07	5.80	0.03
			opx	C		1.82	1.08E-07	5.47	0.10
C273Q	Oku	lherzolite	opx	A		1.54	1.41E-08	4.62	0.18
			opx	B		3.00	1.57E-08	6.51	0.08
			cpx			1.32	7.91E-08	6.65	0.22
C39B	Mt. Cameroon	lherzolite	opx			0.16	2.25E-08	4.23	0.17
			cpx			2.04	2.54E-08	4.38	0.06
Lavas									
R14	Mt. Cameroon	picrite	olv	A		0.19	4.10E-07	5.41	0.04
			olv	B	1	0.69	4.62E-07	5.25	0.16
					2		2.42E-07	5.15	0.14
			olv	C		2.01	3.37E-07	5.40	0.01
C30	Mt. Cameroon	basanite	olv			2.48	4.99E-09	5.33	0.12
C247	Manengouba	hypersthene normative basalt	olv	A		0.14	5.95E-08	6.46	0.17
			olv	B		0.90	5.11E-08	6.85	0.07
ST72*	São Tomé	basanite	cpx			0.14	4.45E-09	5.88	0.17
ST106*	São Tomé	alkali basalt	olv			0.09	3.79E-09	7.14	0.28
ST115*	São Tomé	alkali basalt	olv	A		0.15	1.34E-08	5.92	0.14
				B		0.15	1.68E-08	5.91	0.09
Carbon dioxide gases									
ST-F2	São Tomé						3.05E-09†	6.97	0.11
ST-F3	São Tomé						4.69E-05†	6.25	0.01
ST-F4	São Tomé			A	1		3.48E-06†	6.43	0.01
					2			6.43	0.01
Standard samples									
2πD43	13.5° N, Mid-Atlantic Ridge	MORB	glass	A	1	0.95	1.85E-06	8.51	0.02
					2		1.22E-07	8.36	0.09
					3		1.54E-07	8.47	0.07
2πD43‡			glass		1	0.94	9.10E-05	8.47	···
					2	1.41	8.30E-05	8.16	···
Re 496	Réunion	dunite xenolith	olv			0.50	3.07E-07	12.32	0.27
Re 496§			olv	1800°C		6.63	2.35E-09	13.1	1.8
				700°C			2.19E-07	12.9	2.3

Read 2.97E-07 as 2.97×10^{-7}. Abbreviations are cpx, clinopyroxene; olv, olivine; opx, orthopyroxene.
*Analyses performed by M. Kurz, Woods Hole Oceanographic Institution: see *Kurz et al.* [1996] for analytical details.
†[^{4}He] cm^3 STP/cm^3 gas.
‡Reported as average isotopic compositions from multistage crushing analysis [*Moreira et al.*, 1998].
§Analysis by stepwise heating at 700 and 1800°C [*Kaneoka et al.*, 1986].

$\pm1\sigma$ for both of the samples (2πD43 [*Moreira et al.*, 1998] and Re 496 [*Kaneoka et al.*, 1986]). Furthermore, our data for Re 496 (12.32 ± 0.27) are similar to other values reported for Réunion [*Staudacher et al.*, 1986; *Graham et al.*, 1990].

4. Results

4.1. Helium

Ultramafic xenoliths in the continental sector of the Cameroon line are characterized by relatively low ^{3}He/^{4}He, ranging from 4.2 to $6.7R_a$, with most $>5R_a$ (Figure 2 and Table 1). Individual phases yield relatively uniform He isotopic compositions for a given xenolith. This relationship is best illustrated by sample C235D where the analyses of olivine, orthopyroxene, and clinopyroxene are identical within error (1σ), regardless of total gas content (Figure 3). Isotopic homogeneity over a wide range of gas contents rules out significant addition of cosmogenic or radiogenic He following the formation of fluid inclusions in the mantle.

We selected a suite of young (<5 Ma) lavas, with high MgO content (≥8% MgO), for helium isotopic analysis [*Lee et al.*, 1994; *Halliday et al.*, 1990; *Barfod*, 1999]. High MgO lavas are unlikely to have undergone extensive differentiation within the crust and so are less likely to have been contaminated by crustal noble gases. The helium isotopic compositions of these samples range from 5.1 to 7.1R_a. Multiple-step crushing of sample R14 revealed isotopic equilibrium for two successive crushing steps. This sample is isotopically identical to the related R56 xenolith sample; the two were obtained from the same flow and are probably genetically related. The He isotopic compositions of the lavas are broadly similar to those measured for the bulk of the xenoliths but do not range to the lower values observed in the xenoliths.

Carbon dioxide fluids collected from springs on the island of São Tomé have uniform He isotopic compositions ranging from 6.25 ± 0.01 to 6.97 ± 0.11R_a (Figure 2). These compositions overlap the upper range observed in xenoliths and lavas. The gases measured in these samples are dominated by CO_2 (76%), along with O_2 (3.5%) and N_2 (13%); the remainder is probably water vapor. The ratios of $CO_2/^3He$ are 1.8×10^9 and 2.4×10^{10} for samples ST-F3 and ST-F4, respectively, similar to the range of values observed for MORB and ocean island xenoliths [*Marty and Jambon*, 1987; *Trull et al.*, 1993]. Sample ST-F2 appears to be depleted in noble gases (or enriched in CO_2). Lack of correlation between Ar or Ne with He isotopes in the fluid samples indicates that air contamination did not significantly lower the He isotopic compositions.

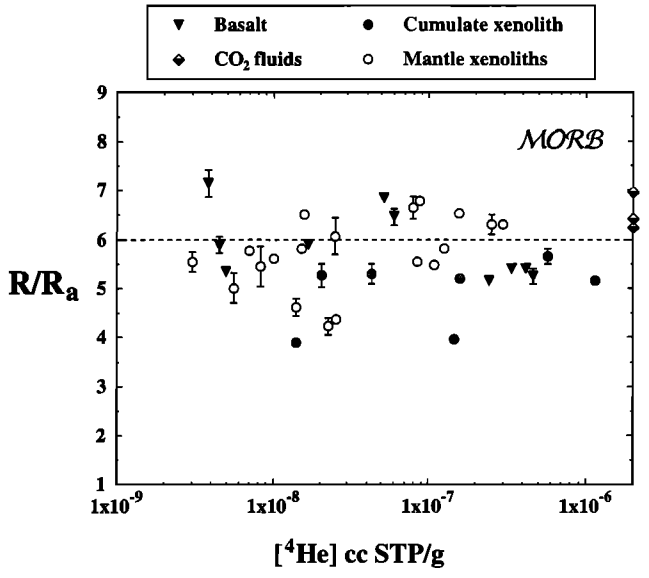

Figure 2. A summary diagram of He isotopic data from the Cameroon line (this study) plotted against ^4He concentration. Data for silicates (basalts, mantle xenoliths, cumulate xenolith) span ~3 orders of magnitude in gas concentration. The gas concentration does not show a simple correlation with isotopic composition, suggesting that the samples possessing low gas concentrations have not been significantly modified by postemplacement processes such as radiogenic or cosmogenic additions. Data for CO_2 fluids are plotted along the left-hand side for the purpose of comparison. All data are plotted with 1σ errors for the isotopic composition. Most of the data fall between 5.0 and 6.5R_a. The horizontal dashed line is a 6R_a reference line.

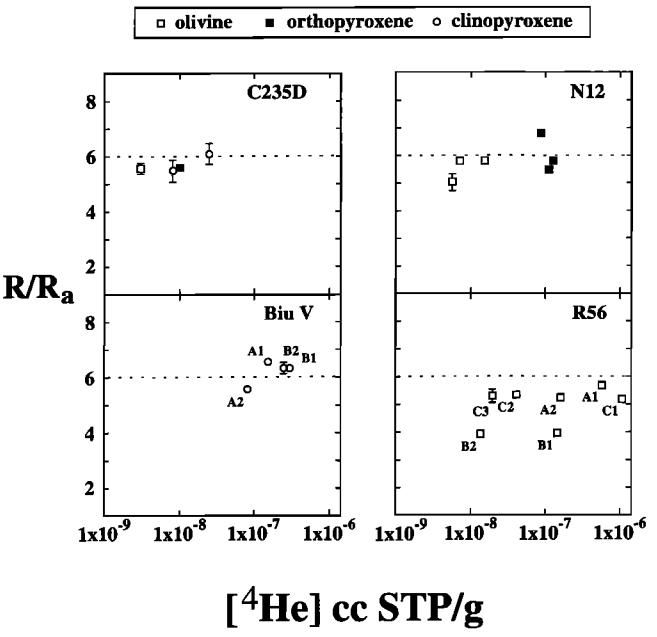

Figure 3. Helium isotopic compositions and He concentrations of individual xenolith samples, plotted along with the 6R_a reference line. Samples C273Q, C39B, C235D and N12 have analyses of different mineral phases which typically span a wide range of gas concentrations, but in general, these individual analyses are in isotopic equilibrium for a given sample. The presence of isotopic equilibrium on the mineral scale argues strongly that these samples have not been affected by postemplacement modification of the isotopic compositions. Samples Biu V and R56 have been analyzed for single phases only (clinopyroxene and olivine, respectively) but have been the subject of multiple-step crushing experiments with little or no isotopic disequilibria between the crushing steps. As with the multiphase analyses, the multiple crushing experiments also suggest an absence of postemplacement modification.

4.2. Neon

Neon isotopic data for four xenoliths from the continental sector are presented in Figure 4 and Table 2. Much of the data lies along or just above the MORB array [*Sarda et al.*, 1988], with maximum $^{20}Ne/^{22}Ne$ and $^{21}Ne/^{22}Ne$ of 11.87 and 0.0508, respectively. These same analyses have He isotopic compositions of 3.96 to 6.54R_a, significantly more radiogenic than average MORB compositions.

Neon data for CO_2 fluids are presented in Figure 4. The data are close to atmospheric or lie just above the MORB array. Helium isotopic data for the fluids show a pattern similar to that of the xenoliths, i.e., more radiogenic than MORB.

4.3. Argon

Argon isotopic data for xenoliths obtained by crushing deviate from the air composition, with $^{40}Ar/^{36}Ar$ ranging from 1220 to 4910. Argon data show no correlation with Ne or He isotopes. Data for lava R14 olivine (crushing) are similar to the range observed in the xenolith samples. CO_2 fluids range from $^{40}Ar/^{36}Ar$ of 288 to 1650 and show a positive correlation with Ne isotopes. This is consistent with the addition of 70–80% of an atmospheric component to mantle-derived gases that have a minimum $^{40}Ar/^{36}Ar$ of 1650 (Figure 5).

Argon isotopic data for single-grain laser heating analyses of phases from xenoliths and a lava are presented in Figure 5 and

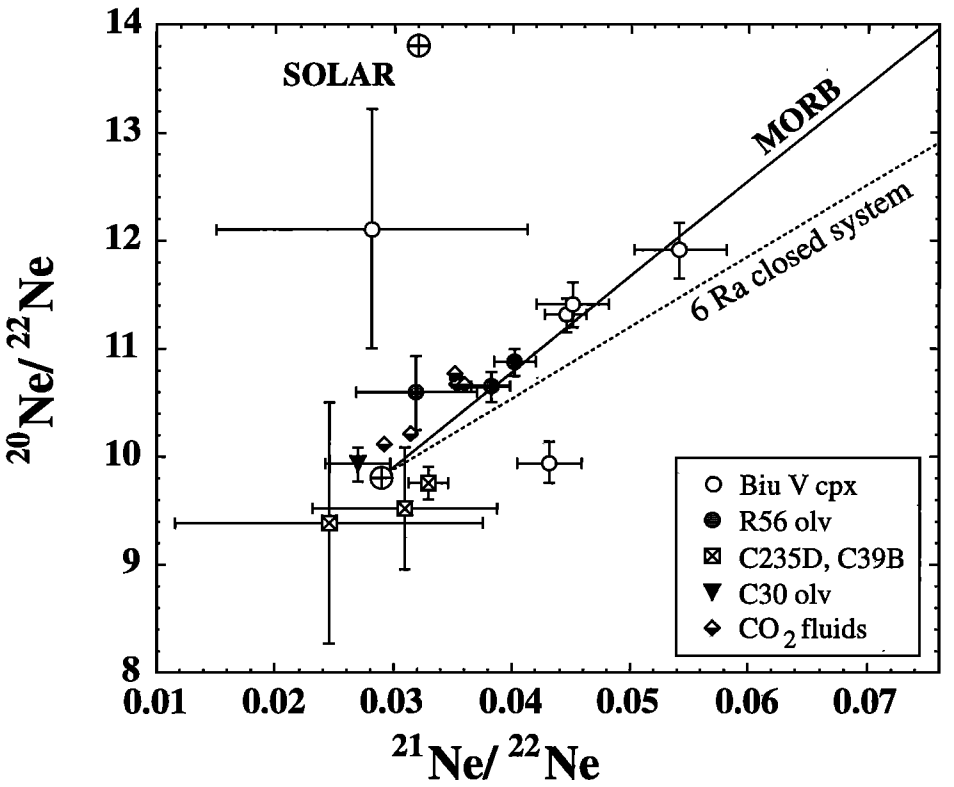

Figure 4. Three Ne isotope data for fluids and silicates from the Cameroon line with 1σ errors. These data are indistinguishable from the MORB array as defined by the data of *Sarda et al.* [1988] and *Moreira et al.* [1998], indicated by the solid line. Data for Ne were obtained from samples spanning the 1600-km Cameroon line (São Tomé, Mount Cameroon, Biu Plateau). Coherency of the Ne and He data, across both the continental and oceanic sectors of the volcanic chain, suggests that these gases have a sublithospheric source. Despite the Cameroon Ne data being MORB-like, the He isotopic data for the same samples are more radiogenic than MORB compositions, suggesting that the source region of the gases has a low time-integrated $^3He/^{22}Ne$ ratio, less than that of the MORB source. A model array for closed-system evolution to $6R_a$ of a mantle reservoir with $^3He/^{22}Ne = 4$ is shown (dotted line).

Table 2. Neon and Argon Data

Sample	Phase	Run	Step	$[^{20}Ne]$ cm^3 STP/g	$^{20}Ne/^{22}Ne$	$\pm1\sigma$	$^{21}Ne/^{22}Ne$	$\pm1\sigma$	$[^{40}Ar]$ cm^3 STP/g	$^{40}Ar/^{36}Ar$	$\pm1\sigma$
Xenoliths											
Biu V	cpx	A	1	1.39E-10	11.30	0.16	0.0445	0.0018	8.14E-06	1220	34
			2	3.55E-11	11.90	0.26	0.0543	0.0039	1.32E-07	3911	341
	cpx	B	1	7.59E-11	9.93	0.19	0.0431	0.0027			
			2	4.63E-11	11.40	0.21	0.0451	0.0031			
R56	olv	A	1	1.33E-10	10.63	0.14	0.0382	0.0016			
			2	2.36E-11	10.57	0.34	0.0319	0.0051			
	olv	B	1	1.22E-10	10.86	0.13	0.0403	0.0017	1.03E-07	1707	179
				4.76E-12	12.10	1.11	0.0282	0.0131			
C235D	cpx			3.92E-12	9.38	1.12	0.0247	0.0130	7.80E-09	1465	36
C39B	opx			1.14E-11	9.51	0.56	0.0311	0.0078	9.81E-09	1377	88
	cpx			4.63E-11	9.74	0.15	0.0330	0.0017	9.04E-08	4916	998
Lavas											
C30	olv			1.47E-11	9.92	0.16	0.0271	0.0027			
Carbon dioxide gases											
ST-F2				3.95E-10*	10.10	0.03	0.0292	0.0003	3.90E-08†	288	2
ST-F3				3.26E-09*	10.19	0.03	0.0315	0.0002	2.96E-07†	656	7
ST-F4		A	1	8.18E-10*	10.64	0.03	0.0354	0.0003	3.70E-07†	1648	21
			2		10.75	0.03	0.0352	0.0004			
ST-F4		B	1	5.48E-10*	10.69	0.07	0.0354	0.0010	5.86E-07†	1579	30
			2		10.65	0.03	0.0360	0.0003			

*$[^{20}Ne]$ cm^3 STP/cm^3 gas.
†$[^{40}Ar]$ cm^3 STP/cm^3 gas.

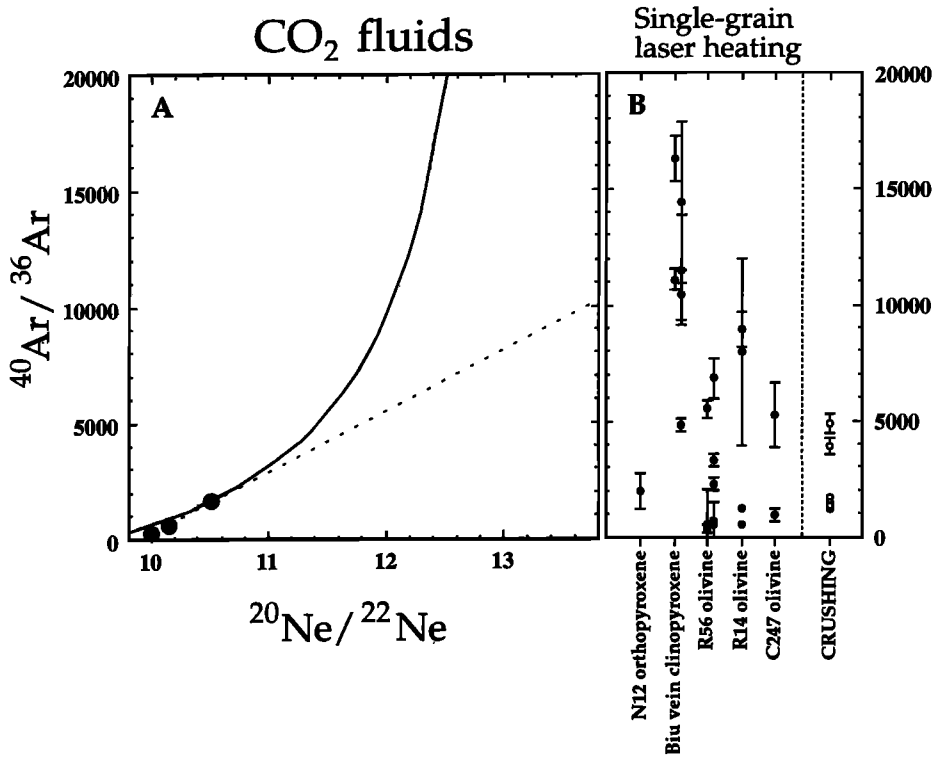

Figure 5. (a) Neon and Ar data for CO_2 fluids from São Tomé. The covariation of the isotopes suggests mixing between an atmosphere-like component (low $^{20}Ne/^{22}Ne$ and low $^{40}Ar/^{36}Ar$) and a mantle-derived component with a minimum $^{40}Ar/^{36}Ar$ of 1650 ± 20. A zero-order assumption is that Ne and Ar are linearly correlated (dotted line), but this is unlikely since it demands that $^{22}Ne/^{36}Ar$ ratios be the same in each reservoir. For example, using an estimate for the mantle of $^{22}Ne/^{36}Ar = 0.25$ [*Porcelli and Wasserburg*, 1995] and an unfractionated atmospheric component with $^{22}Ne/^{36}Ar = 0.053$, the inferred $^{40}Ar/^{36}Ar$ is ~20,000 at $^{20}Ne/^{22}Ne = 12.5$ (solid line), but this estimate has considerable uncertainty due to a lack of data with higher ratios. (b) For comparison, Ar isotopic data for single-grain laser heating and multiple-grain crushing experiments on individual phases from lavas and xenoliths. In a few cases, at high power heating steps, partial fusion was achieved. The sample Biu vein clinopyroxene shows the highest $^{40}Ar/^{36}Ar$ ratios (16,300 ± 1000) and several steps close to 11,000. The $^{40}Ar/^{36}Ar$ data obtained by crushing range between 1000 and 2000, with a few values close to 5000, substantially lower than the upper limits of the laser heating data.

Table 3. The maximum $^{40}Ar/^{36}Ar$ observed is 16,300 ± 1000 for vein clinopyroxene from the Biu xenolith.

5. Characteristic HIMU Noble Gas Isotopic Compositions

The Cameroon line samples are characterized by relatively uniform He isotopic compositions that are similar to, but distinctly lower than, those of MORB. Helium isotopic data for several ocean islands, continental hotspots, specific HIMU systems, and regionally averaged MORB are summarized in Figure 6. The range of He isotopic compositions observed in the Cameroon line is indistinguishable from data for HIMU basalts of the Austral Islands ($5.4–7.6R_a$), St. Helena and ($4.3–5.9R_a$), and Guadalupe ($5.5–5.8R_a$) [*Graham et al.*, 1992; *Eiler et al.*, 1997; *Hanyu and Kaneoka*, 1997]. The data for the Cameroon line and these other HIMU locales are distinct from those of other hotspot systems that typically (with the exception of Réunion) show considerable isotopic diversity.

Both HIMU and MORB He data are relatively radiogenic in comparison to data from most other oceanic hotspots. In addition, our Ne isotopic compositions are indistinguishable from those observed in MORB. This general similarity between MORB and HIMU noble gas isotopic compositions contrasts sharply with lithophile element isotopic compositions. Most strikingly, MORB have Pb isotopic compositions that are among the least radiogenic in oceanic volcanic rocks, whereas HIMU basalts have the most radiogenic Pb. Furthermore, many other OIB with intermediate Pb isotopic compositions possess the least radiogenic He observed in oceanic volcanic rocks [*Hart and Zindler*, 1989].

The majority of noble gas isotopic heterogeneity in OIB is sourced in the convecting mantle. However, the role of crustal or lithospheric contributions is a subject of considerable debate [*Condomines et al.*, 1983; *Hilton et al.*, 1995; *Eiler et al.*, 1997], and these effects must be considered for the Cameroon line. It is simple to demonstrate here that lithospheric contributions are insignificant. In general, the lithosphere is characterized by highly radiogenic $^3He/^4He$ and $^{21}Ne/^{22}Ne$ as observed, for example, in well gases and U-rich minerals. The Cameroon line magmas traverse two types of lithosphere, distinct in both age and composition. Were the lithosphere a significant source of gas, we would expect the two halves of the Cameroon line to have distinct noble gas isotopic compositions. Furthermore, interaction with the lithosphere should produce large and variable shifts in He and Ne toward radiogenic compositions. Although the average $^3He/^4He$ in the con-

Table 3. Laser Ar Data

Sample	Run	Phase	Step	Milliwatts	Mass, g	[^{40}Ar] cm^3 STP/g	^{40}Ar/^{36}Ar	±1σ
Xenoliths								
Biu (vein)	1	cpx	1	2000	0.0032	3.8E-06	11098	434
			2	4000		3.5E-06	16291	967
Biu (vein)	2	cpx	1	1000	0.0058	3.7E-07	14435	3464
			2	3000		3.7E-07	4834	267
			3	4000		5.0E-07	10430	1063
			4	4000		3.2E-07	11503	2378
N12	1	opx	1	2000	0.0089	...	...	...
			2	3000		2.9E-09	...	...
			3	4000		1.5E-08	1954	762
R56	1	olv	1	750	0.0029	7.3E-09	347	169
			2	4000		1.8E-09	497	1555
			3	4000		1.0E-06	5505	368
R56	2	olv	1	2000	0.0075	2.3E-09	656	828
			2	2000		1.5E-08	529	54
			3	3200		1.8E-07	6813	870
			4	4000		6.6E-08	2283	279
			5	4000		1.5E-07	3285	296
Lavas								
C247	1	olv	1	750	0.0053	1.9E-08	968	279
			2	2000		1.0E-07	5240	1387
R14	1	olv	1	1000	0.0036	3.8E-07	513	9
			2	1200		1.0E-07	7940	4043
			3	4000		3.7E-07	1199	18
			4	4000		4.9E-07	8930	742

tinental sector of the Cameroon line is marginally lower than those in the oceanic sector, this effect is small given the potential variability in He isotopic compositions that should result from lithospheric effects. The constancy of Ne isotopes across the entire volcanic line also argues against any significant lithospheric contribution to the noble gas compositions.

To illustrate the significance of the uniformity of helium isotopic composition, it is worth considering the predicted effects of any lithospheric contributions. The ^{238}U/^{3}He in clinopyroxenes in xenoliths of this study, using U concentrations from *Lee et al.* [1996], range from 5 to 10 × 10^8, far higher than estimates for the convecting upper mantle (e.g., 2 × 10^4 to 4 × 10^4 [*O'Nions and Tolstikhin*, 1994]). Using the measured ^{238}U/^{3}He and assuming that diffusive equilibrium is reached, a change from 8 to 5R_a would take place in just 50,000 years. At the depth of the lithospheric mantle (>30 km), He diffusivity should be high. Using several mineral pair thermometers, *Lee et al.* [1996] inferred a range of equilibration temperatures (800–1000°C) for C235D and C273Q. Using a value of 4 × 10^{-14} cm^2/s for helium diffusivity in olivine, appropriate for a xenolith at 900°C (extrapolated from the data of *Trull and Kurz* [1993]), gives a characteristic diffusion distance ($x = \sqrt{Dt}$) of ~250 μm (for 50,000 years). Although grains sizes in these samples typically range from 0.1 to 4 mm in maximum dimension (see the appendix), the fluid inclusions are trapped along secondary fracture planes [*Roedder*, 1984] that traverse individual grains. This reduces the effective grain size for diffusion such that equilibrium between host and inclusions should be reached. In general, the noble gas isotopic compositions of individual phases of the xenoliths are isotopically indistinguishable from CO_2 gases and lavas across the volcanic chain. This suggests that the He and Ne measured in these xenoliths could not have resided in the lithosphere for more than 5 × 10^4 years at the inferred temperatures. There is therefore no doubt that these noble gases have been recently introduced from the asthenosphere.

We therefore use a working average He isotopic composition of 6R_a as characteristic for the Cameroon line HIMU magmas. Other isotopically homogeneous systems, such as the HIMU islands more generally, are also likely to directly reflect asthenospheric mantle source regions without considerable lithospheric contributions. All HIMU islands have He isotopic compositions similar to the Cameroon line samples. It is therefore clear that a hypothesis for the Cameroon line noble gases should also explain the similarity between all such HIMU He isotopic data. The Ne and Ar data presented here are also of direct relevance to other HIMU systems. These are the first clearly resolved HIMU Ne and Ar isotopic features, and meaningful comparisons are unavailable. The MORB-like character of the Ne isotopes indicates a maximum ^{21}Ne/^{22}Ne = 0.059 (at ^{20}Ne/^{22}Ne = 12.5) for the mantle-derived gas component from the Cameroon line. Any model proposed for HIMU genesis must account for both the He and Ne isotopic compositions found in the Cameroon line.

6. Models for HIMU Genesis

Since all of the widely dispersed HIMU ocean islands (Austral Islands, St. Helena, Guadalupe, Cameroon line) share a common, relatively radiogenic He isotopic composition, a common model should apply to their genesis. Models involving crustal recycling into the mantle appear to explain a wide range of geochemical features of OIB [*Hofmann*, 1997]. An alternative set of models accounts for certain geochemical characteristics of OIB by intramantle enrichment processes alone [e.g., *Halliday et al.*, 1988, 1990, 1995; *Sun and McDonough*, 1989]. Attempting to fit noble gases into these geochemical paradigms has been less successful. In particular, few have attempted to account for the He isotopic compositions of HIMU. Here we use the He and Ne isotopic observations for the Cameroon line to test the following types of models: (1) closed-system evolution of recycled oceanic crust, (2) diffusive exchange between recycled oceanic crust and the present-day MORB source mantle, (3) binary mixing between recycled

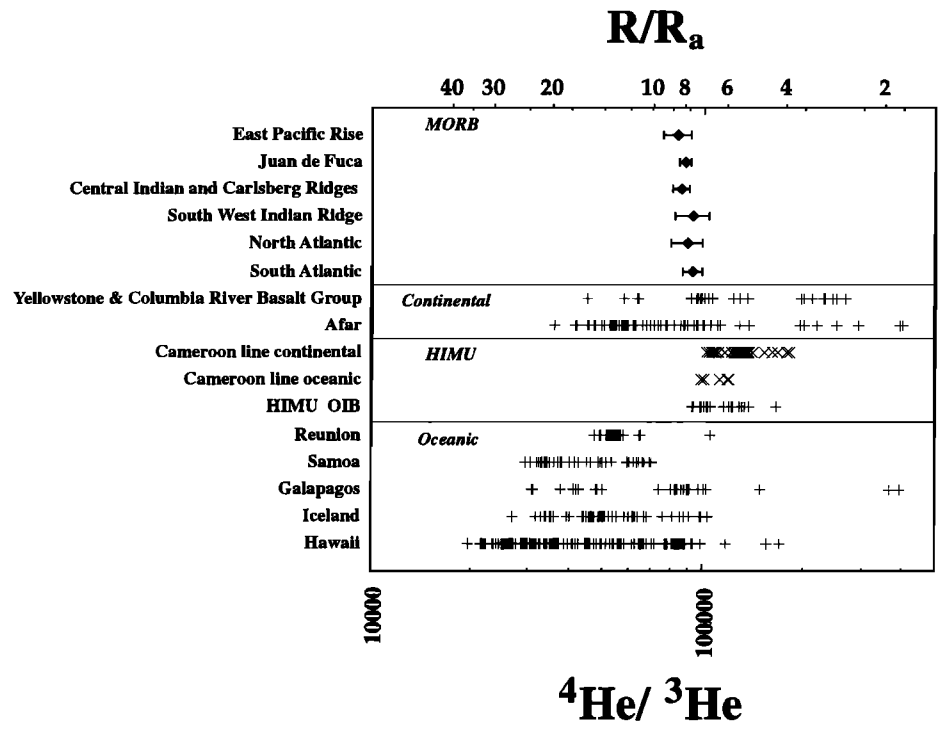

Figure 6. Summary diagram for He isotopic compositions of ocean islands, continental hotspots, the Cameroon line volcanic chain, and MORB. Individual data for both silicates and CO_2 fluids are plotted. The data provide a measure of the heterogeneity of each magmatic system. Data for HIMU OIB and the Cameroon line are relatively homogeneous as compared to the MORB reservoir or to Réunion. The HIMU OIB and Cameroon line are also systematically more radiogenic than either MORB or other OIB. Data sources are Hawaii, *Kyser and Rison* [1982], *Valbracht et al.* [1996], *Staudacher et al.* [1986], *Honda et al.* [1993a], *Rison and Craig* [1983], *Kurz et al.* [1996], *Roden et al.* [1994], *Kurz and Kammer* [1991], *Kurz et al.* [1982], *Craig and Lupton* [1976], *Hiyagon et al.* [1992], *Kaneoka et al.* [1983], and *Kurz et al.* [1983]. Data sources for Réunion are *Staudacher et al.* [1986], *Graham et al.* [1990], *Marty et al.* [1993b], and *Kaneoka et al.* [1986]. Data sources for Samoa are *Farley et al.* [1992] and *Poreda and Farley* [1992]. Data sources for Yellowstone are *Dodson et al.* [1997], *Kennedy et al.* [1987], and *Craig et al.* [1978]. Data sources for Iceland are *Poreda et al.* [1986], *Kurz et al.* [1985], and *Taylor et al.* [1997]. Data source for Galapagos is *Graham et al.* [1993]. Data sources for Afar are *Marty et al.* [1996, 1993a] and *Scarsi and Craig* [1996]. Data sources for HIMU are *Hanyu and Kaneoka* [1997], *Eiler et al.* [1997], and *Graham et al.* [1992]. Compilation of MORB averages and standard deviations by region are from *Allègre et al.* [1995]. Cameroon line is from this study.

oceanic crust and the present-day MORB source mantle, and (4) closed-system evolution of isolated MORB source mantle and Loihi-like mantle (here Loihi-like refers to high $^3He/^4He$ but not to lithophile isotopic compositions).

6.1. Closed-System Evolution of Recycled Crust

The oceanic crust is enriched in U and Th relative to the upper mantle but undergoes severe degassing at plate margins via mid-ocean ridge volcanism, hydrothermal alteration, and dehydration reactions during subduction. Thus the overall (U + Th)/He and (U + Th)/Ne ratios of subducted oceanic crust should be substantially higher than those of other mantle reservoirs. Consequently, recycled slabs should develop highly radiogenic noble gas isotopic compositions on short timescales under closed-system conditions. Figure 7a presents the results of four closed-system calculations for slab material recycled and stored in the mantle for >100 Myr. The calculations assume conservative estimates for U and Th abundances (normal MORB (NMORB) U = 47 ppb, Th = 120 ppb [*Sun and McDonough*, 1989]). To simulate the effect of degassing, we assume a gas content depleted by a factor of ~100 from popping rock concentrations (e.g., 9.9×10^{-10} cm^3 ^{3}He STP/g [*Moreira et al.*, 1998]). These assumptions yield conservative estimates for the effect of degassing; the actual gas contents are probably significantly lower, and therefore the effects on He and Ne isotopic compositions are likely greater [*Staudacher and Allègre*, 1988]. Neon concentrations are varied to give $^3He/^{22}Ne$ initial ratios of 1, 4, and 10. A fourth set of initial concentrations is taken from the He and Ne abundances measured in Jurassic oceanic crust (5×10^{-14} cm^3 ^{3}He STP/g, 8×10^{-12} cm^3 ^{22}Ne STP/g [*Staudacher and Allègre*, 1988]). The $^3He/^4He$ versus $^{21}Ne/^{22}Ne$ evolution for each of these cases, labeled $^3He/^{22}Ne$ = 1, 4, 10, and 0.006 (old crust), respectively, is shown in Figure 7. The time over which the change occurs is indicated exponentially in years on each curve. For lower $^{238}U/^3He$ the rate of isotopic change would be smaller, but the same pathways would be followed. Time increments are directly calculated from U-He systematics.

Neon isotopic change is calculated from ^{4}He production via the $^4He/^{21}Ne$ production ratio (1.5×10^7 [*Ballentine*, 1997]) and $^{21}Ne/^{22}Ne$ production ratios. It is important to note that if a higher estimate of $^4He/^{21}Ne$ production is chosen, e.g., the theoretical estimate (2.2×10^7) of *Yatsevich and Honda* [1997], the arguments for $^3He/^{22}Ne$ fractionation (see below) are

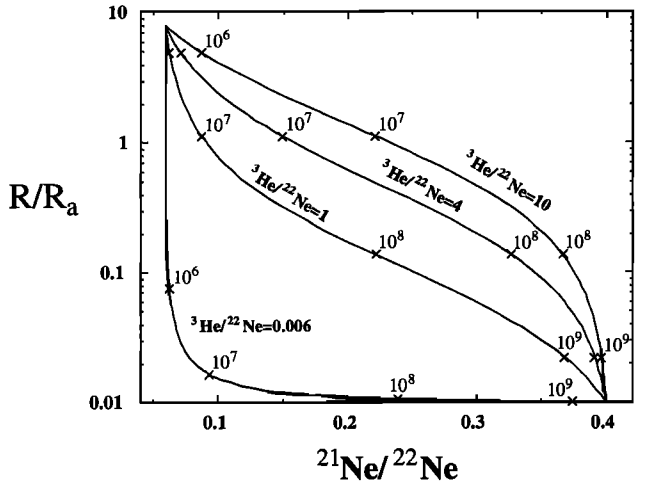

Figure 7a. Closed-system evolution of a basaltic slab. Model calculations assume U and Th abundances of 47 and 120 ppb [*Sun and McDonough*, 1989]. Conservative high estimates of He and Ne abundances are taken from popping rock data, depleted by a factor of 100 [*Moreira et al.*, 1998]. These depleted gas abundances are similar to those found in Jurassic oceanic crust in the Atlantic Ocean [*Staudacher and Allègre*, 1988] and probably represent an upper limit for the noble gas content in recycled oceanic crust. Three curves describe the isotopic evolution of He and Ne with different $^3He/^{22}Ne$ ratios. At these gas abundances and U + Th content the slab rapidly accumulates radiogenic gas. A timescale (in years) is shown on the curves and indicates that the slab will reach the production ratio after an accumulation time in excess of 10^9 years and will exceed the compositions of the Cameroon line data in $\sim 10^6$ years. The closed-system model poses a serious problem since slabs are thought to reside in the mantle for ~1–2 Gyr in order to accumulate sufficiently radiogenic Pb.

weakened. However, use of the higher theoretical value does not affect the conclusions regarding mixing and diffusive equilibration (see below). Our preferred value is based on measurements from several basin fluid studies and is likely the more robust estimate.

In this case we chose a low estimate for the $^{21}Ne/^{22}Ne$ production ratio of 0.4, much lower that the theoretical estimate of 30–40 [*Yatsevich and Honda*, 1997]. Our low estimate is justified by the observation that $^{20}Ne/^{22}Ne$ in MORB has a maximum value of ~12.5, less than solar (13.8) [*Farley and Poreda*, 1993; *Moreira et al.*, 1998; *Barfod*, 1999]. We interpret this feature to reflect enhanced ^{22}Ne production (via $^{19}F(\alpha, n)^{22}Ne$) in the MORB source region, giving a $^{21}Ne/^{22}Ne$ production ratio of ~0.4 [*Niedermann et al.*, 1997; *Moreira et al.*, 1998; *Barfod*, 1999]. A higher ratio only strengthens the arguments below. Because of the enhanced production of ^{22}Ne the $^3He/^{22}Ne$ labels for each curve represent initial, rather than time-integrated, ratios.

The recycled slab is seen to rapidly approach the production ratios of the respective species, irrespective of $^3He/^{22}Ne$ or starting isotopic composition. Any enrichment of U and/or Th in the slab, due, for example, to seafloor alteration [*Hart and Staudigel*, 1989] or more extensive degassing of the slab, will increase the rate at which He and Ne approach production ratios. In addition, considerable radiogenic gas concentrations build up in the slab (irrespective of the particular production ratios chosen), which cannot easily be overprinted by subsequent processes (see below). It has been suggested that subduction zone stripping of incompatible elements, including U, Th, and K, could maintain low $^{238}U/^3He$ ratios and thus preserve primitive noble gas isotopic compositions of recycled materials [*Albarède*, 1998]. Although loss of Th and especially U from subducted materials is an important process recognized in arc volcanism, it remains uncertain to what degree recycled materials are depleted in lithophile trace elements and whether some of these losses may be balanced by earlier enrichments, e.g., U addition due to seafloor weathering [*Hart and Staudigel*, 1989]. Furthermore, the Nb/U ratio of OIB indicates little loss of U during subduction. In contrast, the net loss of primordial noble gases is unequivocally predicted. Therefore, if closed-system slabs are the source of HIMU OIB, the expected noble gas isotopic compositions should be extremely radiogenic. This is not observed. Closed-system slab recycling models do not account for the He and Ne isotopic compositions of HIMU OIB.

6.2. Diffusive Exchange Between Slab and Ambient Mantle

Extensive diffusive exchange of He between the slab and the ambient mantle has recently been proposed as a mechanism for generating HIMU sources with isotopic ratios of $\sim 6.8R_a$ [*Hanyu and Kaneoka*, 1998]. Their model calculations employ a Fourier transform solution to the diffusion equation in an infinite slab or a sphere, with a source term for production of ^4He. The initial conditions are based on the assumption that ^3He in the slab is completely equilibrated with the convecting mantle (their effective "open-system" model). Therefore the model is independent of the initial composition of the recycled slab. The model allows the exploration of the effects of timescale of storage, slab thickness, and U (+Th) content of the slab. *Hanyu and Kaneoka* [1998] assert that recycled ocean crust must be attenuated, i.e., the slab thins, to accommodate the characteristic diffusion distance at reasonable U contents. They balance these parameters to predict a length scale of ~1 km for the HIMU source region in the Austral Island chain that reproduces their average $R/R_a = 6.8$ [*Hanyu and Kaneoka*, 1997].

The uniformity of all HIMU OIB therefore requires a similar length scale and age for all HIMU sources. Processes leading to slab attenuation might be expected to produce a wide range of length scales (thicknesses) in the mantle. Variable but long storage times and variable parent element concentrations would also result in a broad range of noble gas isotopic compositions. A simple open-system diffusion model does not account for the uniform $^3He/^4He$ observed because of the multiple parameters that must be balanced to produce this composition.

Additional uncertainty in a rigorous treatment of noble gas diffusion in the mantle arises from the lack of knowledge regarding the combined pressure and temperature dependence of diffusion at high pressure and temperature. Experiments addressing noble gas diffusion in crystalline silicates are few [*Hart*, 1984b; *Trull et al.*, 1991; *Trull and Kurz*, 1993] and were all performed at atmospheric pressure. However, theoretical and experimental evidence exists supporting pressure dependence of diffusivity in general. Experiments by *Roselieb et al.* [1996] show a decrease in Ar diffusivity in jadeite melt from a log D of approximately −9.15 to −9.48 in samples synthesized at pressures ranging from 0.2 to 6 kbar. Molecular dynamics simulations [*Bryce et al.*, 1997] indicate a positive activation volume for Na, with D_{Na} decreasing ~2 orders of magnitude

over 25 GPa. However, experiments on Ca diffusion in silicate melts indicate a temperature-dependent decrease in activation volume over a pressure range from 0.1 to 3 GPa [*Watson*, 1979]. The diffusivity of He and Ne in the mantle may therefore be less than that determined at low pressure at a given temperature, but this effect may or may not be entirely compensated by the concomitant temperature increase with depth [*Watson*, 1981].

Irrespective of these uncertainties, Ne data from the Cameroon line place additional constraints on a diffusive exchange model. Because the atomic volume of Ne is at least 40% greater than that of He (sixfold coordination [*Zhang and Xu*, 1995]), Ne diffusivity is lower than that of He due to the expected higher activation energy of Ne. We can thus examine the combined evolution of the He and Ne isotopic compositions in the context of the diffusive exchange model. For example, if diffusive exchange of He with the MORB source region is sufficiently effective to bring the isotopic ratio of the recycled material to $6R_a$, the exchanged Ne isotopic composition would be more radiogenic than that of a closed-system evolution of MORB at $6R_a$ (Figure 4; see $6R_a$ closed-system line). An extension of the Hanyu and Kaneoka model (slab geometry) to both He and Ne is shown in Figure 7b. The Cameroon line Ne isotopic data can be considered a two-component mixture of air and mantle derived end-members. With air $^{20}Ne/^{22}Ne = 9.80$ and mantle $^{20}Ne/^{22}Ne = 12.5$ the $^{21}Ne/^{22}Ne$ of the samples can be corrected for air contribution to give the HIMU source $^{21}Ne/^{22}Ne$ (Figure 7b). These values can be directly compared to the model results.

In all calculations, initial U = 50 ppb and Th/U = 2.9 [*Sun and McDonough*, 1989]. The concentrations of gases in the upper mantle are $^3He = 1.15 \times 10^{-11}$ cm^3/g and $^{22}Ne = 2.57 \times 10^{-12}$ cm^3/g; these estimates are based upon a whole mantle steady state model [*Porcelli and Wasserburg*, 1995]. The preferred value for ^{3}He concentration is slightly less than estimates based on mid-ocean ridge fluxes of ^{3}He [*Craig et al.*, 1975; *Farley et al.*, 1995] and ocean crust production rates, e.g., $^3He = 3.4 \times 10^{-11}$ cm^3/g [*Kellogg and Wasserburg*, 1990]. Therefore our estimates of noble gas abundances are reasonably secure to within an order of magnitude.

Three evolution curves that terminate at 2 Gyr (dotted lines) are shown for diffusively exchanging slabs. To be consistent with *Hanyu and Kaneoka* [1998], our extension of the diffusive exchange model also specifies that nonradiogenic noble gases in the slab (e.g., ^{3}He, ^{20}Ne) are in equilibrium with the ambient mantle. Accumulation and diffusive loss of radiogenic ^{22}Ne, ^{21}Ne, and ^{4}He are accounted for by the calculations. It is also assumed that Ne diffusion is 10 times slower than that of He [*Ozima and Podosek*, 1983]. Three cases are considered here for illustration: curve A, "fast" ^{4}He diffusion ($D_{He} = 10^{-4}$ cm^2/s), used by *Hanyu and Kaneoka* [1998] for grain boundary diffusion at 1600°C and 300 m for the thickness of the slab; curve B, "slow" ^{4}He diffusion ($D_{He} = 10^{-6}$ cm^2/s, volume diffusion) and 300 m slab thickness, and curve C, "slow" ^{4}He diffusion ($D_{He} = 10^{-6}$ cm^2/s) and 100 m slab thickness.

The results of the diffusion models are shown in Figure 7b. Solid lines show closed-system evolution results from Figure 7a for reference. The He-Ne isotopic evolution in the open system model is highly dependent on the magnitudes of the diffusion coefficients. As the diffusivities of He and Ne decrease, the pathways approach the closed-system behavior. Higher diffusion coefficients result in more rapid loss and exchange of accumulated radiogenic He and Ne (curve A) than the lower

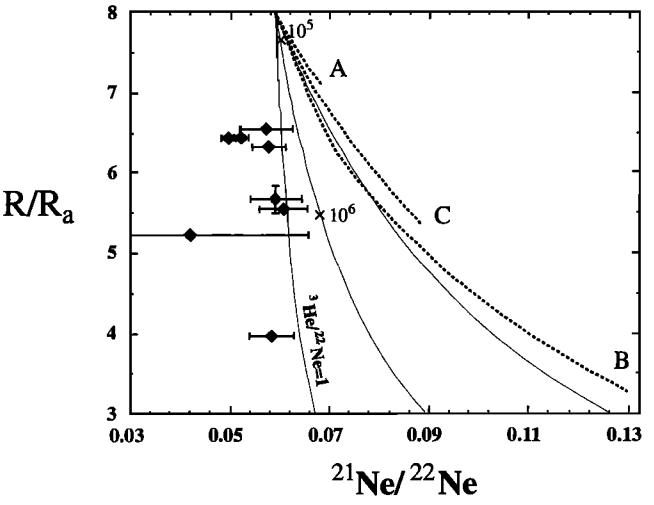

Figure 7b. Diffusive exchange in recycled oceanic crust. Thin solid lines represent the closed-system model (enlargement from Figure 7a, linear scale). Diamonds are Cameroon line data with air-corrected $^{21}Ne/^{22}Ne$ (extrapolated to $^{20}Ne/^{22}Ne = 12.5$) plotted versus He isotopic data (1σ errors). The dotted lines (curves A, B, and C) are model calculations for a diffusively exchanged slab, using the model of *Hanyu and Kaneoka* [1998] over a 2-Gyr period. The diffusion calculations assume a U content of 50 ppb and Th/U ratio of 2.9. Upper mantle ^{3}He and ^{20}Ne concentrations are from *Porcelli and Wasserburg* [1995]. Ingrowth and diffusive loss of ^{4}He, ^{21}Ne, and ^{22}Ne are determined. Curve A assumes diffusivities of $D_{He} = 10^{-4}$ and $D_{Ne} = 10^{-5}$ and a slab thickness of 300 m. Curves B and C assume diffusivities of $D_{He} = 10^{-6}$ and $D_{Ne} = 10^{-7}$, curve C is for a 100-m slab thickness, and curve B is for a 300-m slab thickness. At these diffusivities and timescales the assumption of isotopic equilibrium between slab and ambient mantle is valid for nonradiogenic isotopes (e.g., ^{3}He, ^{20}Ne). Each calculation (or curve) terminates at 2 Gyr. The models suggest that overall the compositions become less radiogenic with decreasing slab thickness and increasing diffusivity at a given time. However, the relative isotopic composition of Ne is also more radiogenic at a given He isotopic composition for these same parameters; i.e., for curves B and C at $6R_a$ the thinner slab has more radiogenic Ne (albeit the thinner slab is older).

diffusion coefficients which result in greater accumulation of radiogenic gases within the slab (curve B). The loss of ^{4}He compared with ^{21}Ne and ^{22}Ne is more important with increasing diffusion coefficient, resulting in more radiogenic $^{21}Ne/^{22}Ne$ relative to $^3He/^4He$. Reducing slab thickness is analogous to increasing the diffusivity and results in a trajectory similar to that of the high-diffusivity case (curve C). With decreasing diffusion coefficients the slab material achieves more radiogenic Ne and He isotopic compositions overall at given U + Th contents, time intervals, and thicknesses.

It is not possible to obtain He isotopic compositions similar to those of the Cameroon line within the open-system model without also developing Ne isotopic compositions more radiogenic than those observed (Figure 7b). Although the trajectories of the different models tend toward the observed data with decreasing diffusivities, the limiting case of no diffusive exchange (i.e., closed-system model) has already been shown to be untenable for HIMU genesis.

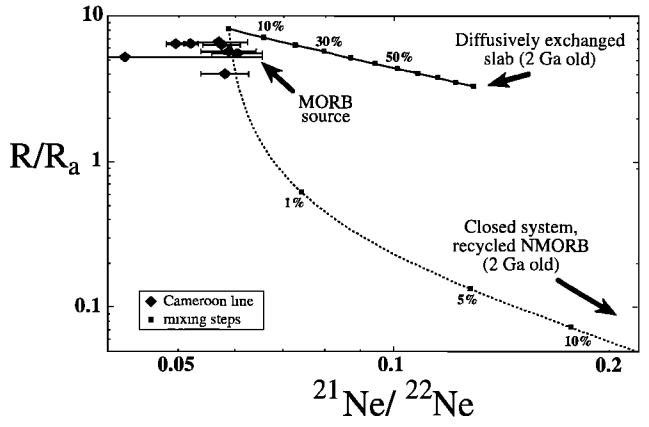

Figure 8a. Binary He-Ne isotopic mixing model for 2-Gyr recycled basaltic crust admixed to MORB source mantle. Diamonds indicate Cameroon line data; the $^{21}Ne/^{22}Ne$ ratios are air-corrected mantle components (1σ errors) assuming $^{20}Ne/^{22}Ne = 12.5$. Numbers along the curves (squares) show percentage mixing steps for admixture of closed system (dotted line) and diffusively exchanged (solid line) slab. See text for discussion.

6.3. Mixing Between Slab and Mantle

Mixing of upper mantle with recycled slab material has been proposed to explain the lithophile isotopic and trace element composition of OIB in the Austral Island chain. *Chauvel et al.* [1992] favor a binary mixing model involving ~25% admixture of ancient recycled oceanic crust to a 75% remainder of upper mantle peridotite. However, mixing of MORB source mantle with highly radiogenic recycled material (Figure 7a) might be expected to produce a broad array of noble gas isotopic compositions. The relative uniformity observed in the Cameroon line and other HIMU OIB therefore places stringent requirements on the mixing mass balance. The $^3He/^4He$ of HIMU is close to that of MORB, rather than being highly radiogenic, demanding a dominant MORB source component. In contrast to He, the Ne isotopic compositions are not intermediate between MORB source and slab compositions but instead have MORB-like compositions. This places strong constraints on the range of possible He/Ne of each end-member in any two-component mixing scenario.

We examine three mixing scenarios; modern MORB-source admixed with (1) a 2.0-Gyr closed-system slab composition from Figure 7a, $R/R_a = 0.01$, $^{21}Ne/^{22}Ne = 0.4$, (2) a 2.0-Gyr diffusively exchanged slab from Figure 7b (model B); $R/R_a = 3.3$, $^{21}Ne/^{22}Ne = 0.13$, and (3) a 2.0-Gyr closed-system slab composition with reduced U + Th content to simulate subduction zone removal of large ion lithophile elements (factor of 100 from NMORB compositions, i.e., 0.47 ppb U, 1.2 ppb Th); $R/R_a = 0.53$, $^{21}Ne/^{22}Ne = 0.216$. In these models, MORB-source isotopic compositions are $8R_a$ and $^{21}Ne/^{22}Ne = 0.059$. Helium and Ne abundances for the MORB source are 1.15×10^{-11} cm^3 STP/g ^{3}He and 2.57×10^{-12} cm^3 STP/g ^{22}Ne [*Porcelli and Wasserburg*, 1995]. The gas content of the closed-system slab are 2.78×10^{-11} cm^3 STP/g (^{3}He) and 2.13×10^{-10} cm^3 STP/g (^{22}Ne), taken from the calculations presented in the closed-system evolution section. The abundance of ^{3}He in the diffusively exchanged slab is equivalent to the MORB source values (see section 6.2), and ^{22}Ne is taken from the diffusive exchange calculation (3.23×10^{-12} cm^3 STP/g). Gas concentrations of ^{3}He and ^{22}Ne for the low U + Th slab are 1.01×10^{-11} cm^3 STP/g and 4.57×10^{-12} cm^3 STP/g, respectively. The abundance of ^{3}He in the closed-system slabs is elevated with respect to initial concentrations (9.9×10^{-12} cm^3 STP/g ^{3}He) because of the small but finite production of ^{3}He by (n, α) reactions on ^{6}Li in the mantle over 2 Gyr [*Ozima and Podosek*, 1983]. The choice of a low $^{21}Ne/^{22}Ne$ production ratio (0.4) leads to enhanced ^{22}Ne production. However, the mixing mass balance is not affected by this since the increase in ^{22}Ne is compensated by the reduction in the $^{21}Ne/^{22}Ne$ ratio of the slab end-member. Simple binary mixing equations were used to simulate admixtures of recycled material and MORB source mantle and are presented in Figures 8a and 8b along with the Cameroon line He-Ne data.

All three mixing scenarios can recover the He isotopic compositions observed in HIMU and the Cameroon line data. The closed-system slab models (1 and 3) require little input from slab material, <1.0% and <10%, respectively, and pass through the bulk of the Ne data (Figure 8b). The percentage slab contribution for model 3 (reduced U + Th) appears favorable. However, as noted earlier, the original mass balance for HIMU is ~25% slab [e.g., *Chauvel et al.*, 1992], with this estimate being based in part on Pb isotopic constraints. Loss of Pb will accompany removal of U + Th (model 3) and therefore demands a larger contribution from the slab material (>25%) to obtain sufficiently radiogenic Pb in the HIMU source. This in turn violates the noble gas mass balance, generating material via mixing that is too radiogenic to be comparable to the HIMU compositions.

Mixing with diffusively exchanged slab (Figure 8a) can achieve a reasonable mass balance for He (and Pb), with most of the He data recovered at a 20–25% slab contribution. However, the Ne data cannot be recovered and, instead, are too radiogenic owing to the enhanced Ne retention in the slab component.

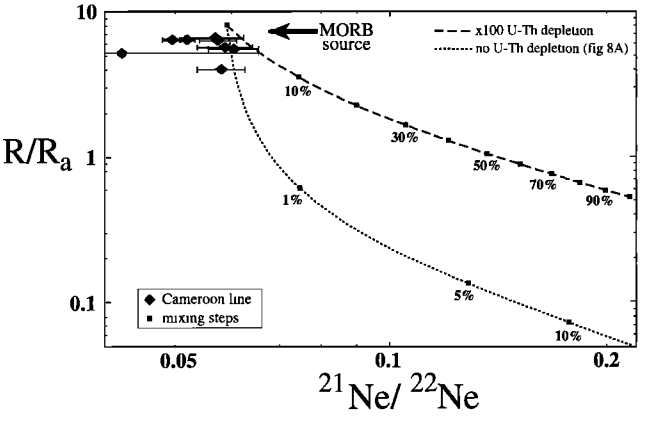

Figure 8b. Extension of the closed-system slab + MORB source mixing model (Figure 8a) with the additional parameter of U + Th stripping from the slab. Uranium and Th are lost initially (to simulate subduction zone processes). This model provides a test for the hypothesis that primordial noble gas compositions can be preserved in subducted slabs over gigayear timescales. Although U + Th loss from slabs, along with subsequent admixture to MORB source mantle can achieve relatively nonradiogenic noble gas isotopic compositions, the mass balance constraints from the Pb isotopic system are severely compromised, making this hypothesis untenable. See text for discussion.

The mixing models above fail to provide the appropriate noble gas isotopic compositions because of improper mass balances and end-member compositions. These arguments illustrate the power of combined observations from the He, Ne, and Pb isotopic systems. Simple, binary mixing processes involving recycled materials and MORB source mantle alone cannot generate HIMU noble gas isotopic compositions. However, if the Pb isotopic constraints are relaxed such that <0.5% recycled slab were required to generate the HIMU Pb isotopic compositions, then a mixing process would be viable.

6.4. Intramantle Processes

Intramantle processes may be the dominant pathways leading to the development of certain features of HIMU chemical and isotopic compositions, regardless of whether or not the ultimate origin of much of the material is recycled slab [*Halliday et al.*, 1995]. First, we discuss isotopic evolution of isolated MORB source and of isolated Loihi-like plume source mantle. We then demonstrate the requirement of $^{3}He/^{22}Ne$ fractionation in either scenario to produce the observed pattern of He and Ne isotopic ratios in HIMU and, finally, discuss potential mechanisms capable of producing the inferred noble gas fractionation.

An intramantle model must specify four parameters to obtain the Cameroon line He and Ne isotopic compositions: (1) initial $^{3}He/^{4}He$ and $^{21}Ne/^{22}Ne$, (2) time-integrated $^{3}He/^{22}Ne$, (3) time-integrated (U + Th)/^{3}He (and hence (U + Th)/^{22}Ne), and (4) timescale. Valid models should not only reproduce the data but should also be predictive of such features as the global occurrence of radiogenic and uniform $^{3}He/^{4}He$ in HIMU volcanic rocks [*Hanyu and Kaneoka*, 1997].

Simple isolation of the MORB mantle has the potential to produce a relatively uniform noble gas source with a $^{3}He/^{4}He$ ratio lower than that of MORB. Taking MORB source $^{3}He = 1.15 \times 10^{-11}$ cm^3 STP/g [*Porcelli and Wasserburg*, 1995], and U = 8 to 18 ppb [*Jochum et al.*, 1983; *White*, 1993], yields estimates of $^{238}U/^{3}He$ (atomic) between 6.5×10^{4} and 1.5×10^{5}. These estimates are consistent with values of $^{238}U/^{3}He = 2 - 4 \times 10^{4}$ from *O'Nions and Tolstikhin* [1994] and require timescales of isolation between 0.1 and 1.0 Gyr to produce a decrease from 8 to $6R_a$. However, it should be noted that the MORB source region was likely less radiogenic ($>8R_a$) at 1 Gyr.

Neon data from the Cameroon line are indistinguishable from MORB but are associated with He that is significantly more radiogenic than MORB. The MORB source has $^{3}He/^{22}Ne$ of ~4 [*Honda et al.*, 1993b; *Honda and McDougall*, 1997]. The isotopic evolution curves for initial values of $^{3}He/^{22}Ne = 4$ (Figure 7a) cannot reproduce the Cameroon line data. This suggests, if such a model is correct, that the Cameroon line source region must have a low time-integrated $^{3}He/^{22}Ne$ (<1) relative to the MORB source region. However, the requirement of a low $^{3}He/^{22}Ne$ could be relaxed if ancient MORB source (e.g., at 1 Gyr) is the starting material. This is because a more primitive composition requires less fractionation of the $^{3}He/^{22}Ne$ ratio. Such a model would be akin to the plume isolation model outlined below but requires a relatively high gas content (low (U + Th)/^{3}He and (U + Th)/^{22}Ne) to slow the change in $^{3}He/^{4}He$ and $^{21}Ne/^{22}Ne$ over 1 Gyr.

Accumulation of radiogenic Ne and He in an isolated plume can provide the necessary compositions, although $^{3}He/^{22}Ne$ fractionation from solar values may still be required (Figure 9). A model advocating aged plume material is in accord with earlier models that explain spatial zonation in $^{206}Pb/^{204}Pb$ and large increases in $^{206}Pb/^{204}Pb$ versus $^{207}Pb/^{204}Pb$ of young basaltic rocks by Mesozoic plume impingement beneath Gondwana [*Halliday et al.*, 1988, 1990; *Lee et al.*, 1994]. In these models the timescale of plume material isolation is thought to relate to that of the breakup of Gondwana, i.e., ~10^{8} years.

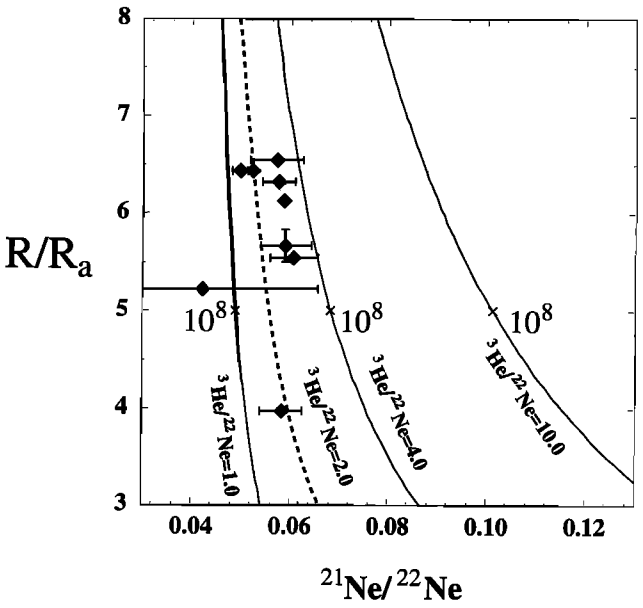

Figure 9. Helium and Ne isotopic plot, similar to Figure 7b, showing the plume head isolation model. Plume material has Loihi-like initial He and Ne isotopic compositions ($32R_a$, $^{21}Ne/^{22}Ne = 0.042$) and gas content reduced by a factor of 2 from popping rock concentrations (i.e., $^{4}He = 1 \times 10^{-5}$ cm^3 STP/g). Three solid curves delineate evolution curves with $^{3}He/^{22}Ne = 1$, 4, and 10. Tick marks show isotopic composition at 10^{8} years. Dashed curve is generated with $^{3}He/^{22}Ne = 2$. The Cameroon line data are shown as in Figure 7b resolved into mantle components (1σ errors). The Cameroon line data are reproduced with $^{3}He/^{22}Ne$ between 2 and 3.

Initial plume composition is isotopically primitive, with Loihi-like He ($32R_a$) and Ne ($^{21}Ne/^{22}Ne = 0.042$). The He concentration is 2.5×10^{-10} cm^3 ^{3}He STP/g (factor of 4 reduction from popping rock concentrations [*Moreira et al.*, 1998]). Uranium and Th concentrations are 21 ppb and 80 ppb, respectively (primitive mantle compositions of *Sun and McDonough* [1989]). The isolated plume material achieves $6R_a$ in ~10^{8} years (indicated in Figure 9). Neon concentrations and isotopic evolution are set by specifying the initial $^{3}He/^{22}Ne$ ratios. The Cameroon line He and Ne data are reproduced with $^{3}He/^{22}Ne$ ~2.

Although either isolation model (MORB source or fossil plume) can produce He and Ne isotopic compositions similar to the Cameroon line data, the fossil plume model does not require extreme $^{3}He/^{22}Ne$ fractionation (i.e., $^{3}He/^{22}Ne$ <1) and is also supported by lithophile radiogenic isotope evidence [*Halliday et al.*, 1988, 1990]. However, closed-system plume isolation is not predictive in the sense that the observed compositions in the Cameroon line are achieved by specific fractionation and ingrowth scenarios, unlikely to be exactly reproduced in the case of other HIMU islands. It is important to note that in the case of the Cameroon line the timescale of fractionation is not constrained by the He-Ne systematics but is inferred from the tectonic history and the Pb isotopic system.

The relevant timescale for the noble gases could thus be considerably longer, and the inferred fractionation could be older and smaller. Because the plume model relies on the geologic circumstances of the Cameroon line, it is not readily applicable to other HIMU ocean islands, e.g., the Austral Islands or St. Helena. However, the processes outlined in this model may be useful in examining the relationship between the Cameroon line and other HIMU centers.

A hybrid model involving both MORB and plume reservoirs may explain the ubiquity of the HIMU He isotopic composition. This model is essentially the same as the plume model above but with one important difference. Here we envisage plume-derived melts trapped in the MORB source asthenosphere. Both the plume-derived material and the MORB source mantle remain convectively isolated over a 10^8 year timescale, developing relatively radiogenic compositions. The trapped melts will exchange diffusively with the ambient mantle reaching near equilibrium in He but not in Ne. Thus the $^3He/^4He$ of the vein would more directly reflect the aged MORB source, whereas the Ne isotopic composition would be somewhat more primitive. All of these intramantle models require $^3He/^{22}Ne$ fractionation for the source of the Cameroon line gases.

7. Helium-Neon Fractionation Processes

As indicated above, the enhanced production of ^{22}Ne (due to the choice of a low $^{21}Ne/^{22}Ne$ production ratio) leads to decreases in $^3He/^{22}Ne$ of a closed system as it evolves. However, on a 10^8 year timescale the reduction is minor compared to the inferred $^3He/^{22}Ne$ fractionation of ~50%. For example, in the case of the plume incubation model the change due to ingrowth in $^3He/^{22}Ne$ is only ~4%. This implies that an additional process must fractionate He from Ne.

Melt-vapor fractionation can fractionate He from Ne, by virtue of the greater solubility of He in melts. It is reasonable to envisage a scenario whereby asthenospheric melts degas into the sublithospheric upper mantle. This would be expected to produce high-pressure CO_2 inclusions in mantle wall rock with low $^3He/^{22}Ne$, complementing a melt with high $^3He/^{22}Ne$ and is a possible explanation for the low mantle $^3He/^{22}Ne$ observed in well gases [*Ballentine*, 1997]. Such a process would be limited to the uppermost mantle given that the requisite vapor phase can only form at relatively low pressures. It is unlikely that a vapor phase can form at depths greater than ~70 km [*Pasteris*, 1987; *Roedder*, 1984]. The similarity of $^3He/^4He$ across both the oceanic and continental sectors of the Cameroon line requires almost no lithospheric contribution and thus indicates a sublithospheric source of the gases. The present-day thickness of the lithosphere beneath the oceanic sector of the Cameroon line can be calculated using a simple half-space cooling model; assuming an age of 100 Ma yields ~100 km as a crude estimate [*Halliday et al.*, 1988]. The thickness of the continental sector will likely exceed this figure. Thus formation of a vapor phase beneath the present lithosphere is considered unlikely. Melt-vapor fractionation as a potential process to generate the required low $^3He/^{22}Ne$ is not discussed further.

On the other hand, melting does occur at sublithospheric depths, and partitioning of He and Ne between melt and solid phases does have the potential to fractionate $^3He/^{22}Ne$. Helium and Ne are incompatible with the major phases of the mantle [*Carroll and Draper*, 1994]. Nevertheless, melt-solid fractionation of He and Ne is poorly constrained by limited and often highly variable experimental and natural partitioning data [*Hiyagon and Ozima*, 1986; *Broadhurst et al.*, 1990; *Carroll and Draper*, 1994]. For example, it is uncertain to what degree $^3He/^{22}Ne$ fractionation can be produced by partial melting. Although this is a promising potential mechanism, we do not pursue it further.

Diffusive exchange processes provide another mechanism by which the noble gases can be fractionated. A simple scenario can be envisaged where a gas-rich region in the mantle (e.g., a pyroxenite vein representing a trapped melt) may diffusively exchange with the surrounding gas-poor mantle. We assume no initial difference in $^3He/^{22}Ne$ between vein and wall rock and a diffusivity of He 10 times faster than that of Ne. We treat ^{22}Ne in this case as nonradiogenic since the ingrowth effect on $^3He/^{22}Ne$ is minor at this time scale. The following solution from *Carslaw and Jaeger* [1959, p. 54] satisfies the boundary conditions for diffusive loss of ^3He and ^{22}Ne from a slab-like body:

$$^3He = \left\{\left[\frac{^3He_{vein} - {}^3He_{mantle}}{2}\right] \cdot \left[\mathrm{erf}\left(\frac{a-x}{2\sqrt{Dt}}\right) + \mathrm{erf}\left(\frac{a+x}{2\sqrt{Dt}}\right)\right]\right\} + {}^3He_{mantle}. \quad (1)$$

Here ^3He_x is the He concentration in the given reservoir, a is the half thickness of the vein, x is distance, t is time, and D is the diffusivity.

The vein would at first be expected to show a decrease in $^3He/^{22}Ne$ as He is lost more rapidly. Eventually, $^3He/^{22}Ne$ would begin to increase and asymptotically approach equilibrium with the wall rock. The time-integrated $^3He/^{22}Ne$ in the vein would be lower than either initial composition. Below, we model this process in the context of the 10^8 year plume fractionation event outlined earlier [e.g., *Halliday et al.*, 1990].

The concentration of ^3He is 1.15×10^{-11} cm^3 STP/g [*Porcelli and Wasserburg*, 1995] for the ambient mantle and 1.15×10^{-9} cm^3 STP/g for the vein region. For both the vein region and surrounding mantle the initial $^3He/^{22}Ne = 4$. We use the "slow" diffusivity of $D_{He} = 10^{-6}$ cm^2/s ($D_{Ne} = 10^{-7}$ cm^2/s). The relationship between time, vein thickness, diffusivity, and the resultant $^3He/^{22}Ne$ is illustrated in Figure 10.

The $^3He/^{22}Ne$ values in each calculation first decrease sharply and then increase toward a value of 4 (the equilibrium value). The minimum $^3He/^{22}Ne$ reached is dependent on the ratio of diffusivities. With increasing difference the minimum is lowered. In this case a value of ~1.4 represents the minimum; for a difference in diffusivity of 2 the minimum is ~2.9. By increasing vein thickness or lowering both diffusivities the minimum is reached later, and the approach to equilibrium is slowed, i.e., 3 versus 300-m thickness at $D_{He} = 10^{-6}$ cm^2/s. For models with thicknesses greater than 3 m the time-integrated $^3He/^{22}Ne$ over the 10^8 year period ranges between 1.5 and 2.5. This result is consistent with the inference of He/Ne fractionation in the Cameroon line data and with the plume ingrowth model presented in Figure 9. The inferred scale length (3–300 m) can be interpreted as a contiguous entity (a solid slab), or it may reflect an aggregate of several smaller veins in a restricted region having an "effective" thickness greater than that of the individual veins. A diffusive exchange mechanism in a veined portion of the asthenosphere underlying the Cameroon line can provide a low time-integrated $^3He/^{22}Ne$ and is fully consistent with previous models of plume storage and incubation.

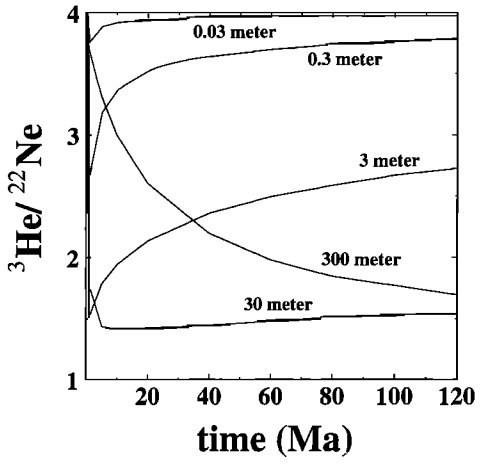

Figure 10. Diffusive exchange of He and Ne from a gas-rich vein (slab) with a gas-poor ambient mantle. Both the vein and surrounding mantle have initial $^3He/^{22}Ne$ = 4, but the gas concentrations in the vein are 100-fold higher. Diffusivity of Ne is assumed to be slower than that of He by a factor of 10. For a slab thickness greater than ~3 m, the time-integrated $^3He/^{22}Ne$ ratio is =2.5 over a 10^8 year period. This degree of He-Ne fractionation is comparable to that inferred from the Cameroon line noble gas isotopic data. The implied length scale may represent a contiguous body (a solid slab 3 m thick) or an "effective thickness" reflecting an aggregate of thinner veins in a restricted region.

8. Conclusions

We have demonstrated that the Cameroon line source region is characterized by relatively uniform He isotopic compositions ($\sim 6R_a$) that are indistinguishable from other HIMU centers but are distinctly more radiogenic than MORB. Neon isotopic compositions are, however, indistinguishable from MORB. The Ar isotopic compositions have a minimum of $^{40}Ar/^{36}Ar$ ~1650 but are as high as ~16,300. The noble gas isotopic compositions are essentially uniform across both the oceanic and continental sectors of the volcanic chain, indicating negligible input of gases from lithospheric sources.

Oceanic crust recycling models involving closed-system slabs and diffusively exchanged slabs, along with mixing of either of these two components with MORB source mantle cannot produce the He and Ne isotopic signatures present in the Cameroon line. This results primarily from the difficulty of producing the Ne isotopic compositions, which are not intermediate between MORB and recycled crust. Loss of U and Th, via subduction zone stripping, cannot ameliorate the problem because of concomitant loss of Pb and the difficulty of recovering the Ne isotopic compositions. Although some closed-system mixing models can reproduce the He-Ne isotopic data, they are not consistent with Pb isotopic constraints.

Isolation of either MORB source or plume source (Loihi-like) mantle can generate the required He and Ne isotopic compositions. However, both models require $^3He/^{22}Ne$ fractionation to values less than solar ($^3He/^{22}Ne$ ~4). Melt-vapor fractionation cannot be invoked. Melt-solid partitioning may provide a simple fractionation mechanism but is unconstrained due to a lack of reliable partitioning data. Diffusive exchange of gas-rich "veins" can generate the inferred magnitude of $^3He/^{22}Ne$ fractionation with reasonable diffusivities of He and Ne and reasonable effective thicknesses.

Following the models of *Halliday et al.* [1988, 1990], we postulate that the noble gas isotopic compositions of the Cameroon line derive from ingrowth in trapped melts from a plume head emplaced into the upper mantle ~10^8 years ago. The isotopic compositions of He and Ne can be achieved in this scenario with reasonable estimates of He and Ne abundance (slightly less than popping rocks) and minor fractionation of He from Ne. Reduction of the time-integrated $^3He/^{22}Ne$ is explained by diffusive exchange of trapped melt veins (the present-day source material) with gas-poor wall rock. Diffusive exchange of noble gases from trapped, plume-derived melts with large reservoirs of aged MORB source mantle may "pin" the He and Ne isotopic compositions to values close to the composition of the MORB reservoir. Although this model may better explain why all HIMU volcanic centers have He isotopic compositions that are close to those of MORB, the ultimate test will lie with acquisition of Ne isotopic data from HIMU locations other than the Cameroon line.

Appendix: Sample Descriptions

A1. Xenoliths

The xenolith samples from this suite were collected in the continental sector of the Cameroon line. Samples C235D, C273Q (protogranular spinel lherzolites), and N12 (porphyroclastic harzburgite) have been described in detail by *Lee et al.* [1996]. Samples C235D and C39B are from a tuff ring surrounding lake Baronbi Mbo, near Mount Cameroon; C273Q is from ~5 km NW of Lake Enep near Oku; N12 and Biu are from the Meringa tuff ring on the Biu Plateau in Nigeria. Sample R56 is a dunite xenolith obtained from basaltic scoria on the Musonge cinder cone (on the flanks of Mount Cameroon; see sample R14 description). See Figure 1b for sample locations.

A1.1. C39B: Spinel lherzolite. Sample C39B is a protogranular [*Mercier and Nicolas*, 1975] spinel lherzolite. Olivine grains are generally equant, range from 0.25 to 4.0 mm, and have straight to curvilinear boundaries with minor subgrain and kink-band formation. Orthopyroxene grains range from 0.25 to 4.0 mm and are unstrained with curvilinear boundaries. Several large orthopyroxene grains show minor exsolution of calcic pyroxene. Clinopyroxene grains range from 0.25 to 1.0 mm and are equant to slightly elongate with curvilinear boundaries. Several grains show minor exsolution of Ca-poor pyroxene. Xenomorphic spinel grains are associated with pyroxenes and range from 125 to 250 μm with rare grains to 3 mm. Spinels have smooth, curvilinear boundaries and are commonly intergrown with clinopyroxene. The mineral mode is 50% olivine, 30% orthopyroxene, 15% clinopyroxene, and <5% spinel. This sample has rare, small patches of localized alteration phases; otherwise, the sample is very fresh.

Fluid inclusions, predominantly in the silicate phases, are fracture controlled, and mostly vermicular in form (up to 5 μm in width). Some equant, spheroidal fluid inclusions (up to 10 μm) are associated with vermicular inclusions. All fluid inclusions form planes that are restricted to single mineral grains.

A1.2. Biu: Amphibole-spinel lherzolite with amphibole-olivine websterite vein. The Biu sample is a composite sample with a band of clinopyroxene-rich material flanked by lherzolite. The clinopyroxene-rich band is interpreted as a vein deposited by the passage of a hydrous basaltic melt [*Irving*, 1980]. Hereinafter, the lherzolitic material is referred to as

"host," and the clinopyroxene-rich material is referred to as "vein."

The host is characterized by a transitional porphyroclastic to mosaic equigranular texture [*Mercier and Nicolas*, 1975]. The vein has a mosaic equigranular texture with no evidence of strain in any of the grains. Both the host and vein have olivine, orthopyroxene, clinopyroxene, spinel, and amphibole in varying proportions; vein 20%, 10%, 70%, ~2%, and ~8% and host 50%, 25%, 20%, ~4%, and ~1%, respectively. In the host, olivine and orthopyroxene are present as large (up to 4 mm), highly strained and kink-banded porphyroclasts and smaller (up to 1 mm) neoblasts with equilibrium triple junctions. Equant to elongate (4 × 1) amphibole (125–750 μm) is present in the host but more abundant in the vein and is associated with spinel (125–1250 μm) and clinopyroxenes (125–1500 μm).

Fluid inclusion shapes include rounded (up to 10 μm) and vermicular (~2 μm) forms. No vermicular inclusions were noted in the host lherzolite. Fluid inclusions are much more abundant in the vein region (>10 times). Some planes of rounded inclusions are seen to crosscut grain boundaries, although this relationship is only seen between like mineral grains and may thus be related to recrystallization. In the vein region, fluid inclusions appear to be restricted to pyroxenes and amphiboles.

A1.3. R56: Dunite xenolith. R56 is dunite xenolith with rare clinopyroxene grains (<5%). The olivine grains have numerous oxide and fluid inclusions which commonly form concentric zones paralleling the olivine grain boundaries. Clinopyroxene in this sample is dissimilar to chromian diopside seen in the lherzolite samples. Given that this sample was erupted from the same vent as the picritic sample R14 (see section A2.1), that the modal abundances of clinopyroxene to olivine in the xenolith and R14 are similar, and that the inclusion textures of R14 and R56 olivine are also very similar, R56 is assumed to be a magma chamber cumulate possibly genetically related or having a petrogenesis similar to that of R14.

A2. Lavas

Sample R14 is from a cinder cone (Mount Musonge) on the flanks of Mount Cameroon. Sample C30 is also from Mount Cameroon. Sample C247 is from north of Mount Koupe, near Manengouba; this sample has previously been analyzed for major and trace elements and for Sr, Nd, and Pb isotopes by *Lee et al.* [1994]. Samples ST72, ST106, and ST115 are from São Tomé; Sr, Nd, and Pb isotopic data for the former two are given by *Halliday et al.* [1990].

A2.1. R14: Hypersthene-normative, olivine-phyric basalt. This sample has 30% olivine, 3% clinopyroxene, 1% oxide, and <1% plagioclase phenocrysts. Olivine phenocrysts are subhedral to anhedral, up to 3 mm in diameter, with abundant oxide, melt, and fluid inclusions. A small fraction of the larger olivine phenocrysts shows kink-banding structures. Clinopyroxene phenocrysts are subhedral to anhedral, range up to 2 mm, and have abundant oxide and fluid inclusions. Oxide phenocrysts are subhedral and range up to 0.5 mm. Plagioclase is present as small (up to 0.6 mm) anhedral shards. Groundmass phases include olivine, clinopyroxene, plagioclase, and oxides, along with large vesicles (~30% by volume).

A2.2. C30: Nepheline-normative ankaramite. The phenocrysts is this sample are olivine (20%) and augite (20%) in subequal proportions. Augite grains are euhedral to subhedral and large (up to 3 mm); some have ragged edges and sieve textures. Most grains are zoned complexly, especially those with large melt inclusions. Olivine grains are large (up to 6 mm) and subhedral. Rare composite olivine grains are present. Both olivine and augite contain variable populations of CO_2, melt, and mineral inclusions. The groundmass is composed of feldspar laths, clinopyroxene, oxides, and olivine, without noticeable glass. Very minor patchy alteration of the groundmass consists of iddingsite on fine grain olivine.

A2.3. C247: Hypersthene-normative basalt. This basalt has 10% plagioclase, 5% clinopyroxene, and 5% olivine phenocrysts. Plagioclase phenocrysts range up to 5 mm and are generally euhedral but have strongly zoned and embayed edges and prominent sieve textures. Plagioclase commonly forms glomerocrysts with clinopyroxene. Clinopyroxene is subhedral to euhedral (up to 2.5 mm), has oxide inclusions, and is often sector zoned and twinned. Olivine (up to 1.5 mm) is subhedral to anhedral and often embayed or skeletal. Olivine phenocrysts have melt inclusions filled with brown glass. Rare xenocrystic quartz grains (up to 0.5 mm) are surrounded by thick reaction rims of acicular pyroxene. The trachytic groundmass has plagioclase, oxides, and clinopyroxene.

A2.4. ST72: Nepheline-normative titanaugite-olivine-hornblende-phyric basalt. The rock contains ~30%, by volume, phenocrysts. Euhedral titanaugite, typically 1 to 3 mm but sometimes up to 8 mm in length, is the most abundant phenocryst phase; olivine and hornblende phenocrysts are less abundant. Euhedral to subhedral and rounded olivine phenocrysts, up to 2 mm long, show slight oxidation to iddingsite around the margins and sometimes along cracks. Hornblende is present as anhedral, partly resorbed phenocrysts up to 3 mm across. Magnetite (up to 0.8 mm) and apatite (hexagonal prisms up to 0.5 mm long and 0.2 mm across) are abundant as microphenocrysts. The groundmass consists of plagioclase laths (up to 0.4 mm long), with granules of augite, magnetite, and iddingsite.

A2.5. ST106: Nepheline-normative olivine-phyric basalt. Olivine is the only phenocryst phase (~20% by volume) and is totally fresh. It ranges in size up to 6 mm; the largest phenocrysts tend to be anhedral, while smaller ones (typically 1 to 3 mm) tend to be euhedral and equant. Some small (<1 mm) phenocrysts are euhedral and elongate. The groundmass is slightly vesicular, very fine grained, and almost opaque, although very small plagioclase laths and elongate crystals of augite are visible.

A2.6. ST115: Nepheline-normative titanaugite-olivine-phyric basalt. Phenocrysts (titanaugite and subordinate olivine) make up ~50% of this highly porphyritic rock. Both phases are euhedral to subhedral; augite phenocrysts tend to be large (up to 8 mm), while the olivine phenocrysts are generally smaller (up to 3 mm). The olivine is altered to smectite around the edges and along cracks. Magnetite forms occasional microphenocrysts (up to 0.4 mm). The groundmass consists of plagioclase laths, augite, magnetite, and smectite.

A3. Carbon Dioxide Fluids: ST-F2, ST-F3, and ST-F4

Carbon dioxide fluids were collected from effervescent groundwater springs (~30°C at time of collection). All springs were located at the northern end of São Tomé, within a few kilometers of geomorphically young cinder cones. The collection device employed an inverted funnel assembly connected via plastic tubing to a 0.5-m section of high-grade copper tubing. Once the assembly had been thoroughly flushed with spring gas (~20 min depending on flow rate), the copper tub-

ing was cold welded at either end to prevent contamination of the sample with atmosphere. Gas compositions for all three samples are ~76% CO_2, ~3.5% O_2, and ~13% N_2 (data from B. Sherwood-Lollar). The remainder (~8.5%) is likely water vapor.

Acknowledgments. The authors would like to thank the people of São Tomé and Príncipe and the people of Annobon, who were very hospitable and helpful during our stay on these islands. The work of Jim Cureton, both before and during our visit to the field, made a rather daunting undertaking as painless as can be imagined in such a remote region. In particular, Larry Barber, Peter Detmer, Angus Gascoigne, and the staff at the Voice of America Relay Station, São Tomé, were exceptionally helpful in providing logistic support, without which our field season in the islands would have been considerably less successful. Additional field assistance on São Tomé was provided by Eugénio Vaz Do Nascimento and Luis Paquete Teixeira (under the direction of Lígia Cristina Soares De Barros) of the Ministry of Natural Resources and Energy. We thank Ken Farley for loan of the solenoid crushing device. Mark Kurz provided three pilot analyses of lavas from the ocean islands (funded by OCE-NSF) and extensive and thoughtful comments on an earlier draft of the manuscript. Thorough and thoughtful reviews by Ken Farley and Bob Poreda are much appreciated. We would also like to thank Mark Rehkämper, Der-Chuen Lee, John Christensen, Becky Lange, and Don Snyder for helpful discussions. This work was funded by NSF grants to C.J.B. and A.N.H. and by the Turner Fund of the University of Michigan to D.B.

References

Albarède, F., Time-dependent models of U-Th-He and K-Ar evolution and the layering of mantle convection, *Chem. Geol.*, *145*, 413–429, 1998.

Allègre, C. J., M. Moreira, and T. Staudacher, $^4He/^3He$ dispersion and mantle convection, *Geophys. Res Lett*, *22*(17), 2325–2328, 1995.

Ballentine, C. J., Resolving the mantle He/Ne and crustal $^{21}Ne/^{22}Ne$ in well gases, *Earth Planet. Sci. Lett.*, *152*, 233–250, 1997.

Ballentine, C. J., D.-C. Lee, and A. N. Halliday, Hafnium isotopic studies of the Cameroon line and new HIMU paradoxes, *Chem. Geol.*, *139*, 111–124, 1997.

Barfod, D. N., Noble gas geochemistry of the Cameroon line volcanic chain, doctoral dissertation, Univ. of Mich., Ann Arbor, 1999.

Ben Othmann, D., W. M. White, and J. Patchett, The geochemistry of marine sediments, island arc magma genesis, and crust-mantle recycling, *Earth Planet. Sci. Lett.*, *94*, 1–21, 1989.

Broadhurst, C. L., M. J. Drake, B. E. Hagee, and T. J. Bernatowicz, Solubility and partitioning of Ar in anorthite, diopside, forsterite, spinel, and synthetic basaltic liquids, *Geochim. Cosmochim. Acta*, *54*, 299–309, 1990.

Bryce, J. G., F. J. Spera, and D. J. Stein, Dependence of self diffusivity on P and T in molten $NaAlSi_2O_6$: Comparison of laboratory and molecular dynamics experiments, *Geophys. Res. Lett.*, *24*(6), 711–714, 1997.

Carroll, M. R., and D. S. Draper, Noble gases as trace elements in magmatic processes, *Chem. Geol.*, *117*, 37–56, 1994.

Carslaw, H. S., and J. C. Jaeger, *Conduction of Heat in Solids*, Clarendon Press, Oxford, England, 1959.

Chase, C. G., Ocean island Pb: Two stage histories and mantle evolution, *Earth Planet. Sci. Lett.*, *52*, 277–284, 1981.

Chauvel, C., A. W. Hofmann, and P. Vidal, HIMU-EM: The French Polynesian connection, *Earth Planet. Sci. Lett.*, *110*, 99–119, 1992.

Condomines, M., K. Grönvold, P. J. Hooker, K. Muehlenbachs, R. K. O'Nions, N. Oskarsson, and E. R. Oxburgh, Helium, oxygen, strontium and neodymium isotopic relationships in Icelandic volcanics, *Earth Planet. Sci. Lett.*, *66*, 125–136, 1983.

Craig, H., and J. E. Lupton, Primordial neon, helium, and hydrogen in oceanic basalts, *Earth Planet. Sci. Lett.*, *31*, 369–385, 1976.

Craig, H., W. B. Clarke, and M. A. Beg, Excess ^3He in deep water on the East Pacific Rise, *Earth Planet. Sci. Lett.*, *26*, 125–132, 1975.

Craig, H., J. E. Lupton, J. A. Welhan, and R. Poreda, Helium isotope ratios in Yellowstone and Lassen Park volcanic gases, *Geophys. Res. Lett.*, *5*(11), 897–900, 1978.

Dodson, A., B. M. Kennedy, and D. J. DePaolo, Helium and neon isotopes in the Imnaha Basalt, Columbia River Basalt Group: Evidence for a Yellowstone plume source, *Earth Planet. Sci. Lett.*, *150*, 443–451, 1997.

Dupré, B., and C. J. Allègre, Pb-Sr isotope variation in Indian Ocean basalts and mixing phenomena, *Nature*, *303*, 142–146, 1983.

Eiler, J. M., K. A. Farley, J. W. Valley, E. Hauri, H. Craig, S. R. Hart, and E. M. Stolper, Oxygen isotope variations in ocean island basalt phenocrysts, *Geochim. Cosmochim. Acta*, *61*, 2281–2293, 1997.

Farley, K. A., Rapid recycling of subducted sediments into the Samoan mantle plume, *Geology*, *23*, 531–534, 1995.

Farley, K. A., and R. J. Poreda, Mantle neon and atmospheric contamination, *Earth Planet. Sci. Lett.*, *114*, 325–339, 1993.

Farley, K. A., J. H. Natland, and H. Craig, Binary mixing of enriched and undegassed (primitive?) mantle components (He, Sr, Nd, Pb) in Samoan lavas, *Earth Planet. Sci. Lett.*, *111*, 183–199, 1992.

Farley, K. A., E. Maier-Reimer, P. Schlosser, and W. S. Broecker, Constraints on mantle ^3He fluxes and deep-sea circulation from an oceanic general circulation model, *J. Geophys. Res.*, *100*(B3), 3829–3839, 1995.

Fitton, J. G., The Cameroon line, West Africa: A comparison between oceanic and continental alkaline volcanism, in *Alkaline Igneous Rocks*, edited by J. G. Fitton and B. G. J. Upton, *Geol. Soc. Spec. Publ.*, *30*, 273–291, 1987.

Fitton, J. G., and H. M. Dunlop, The Cameroon line, West Africa, and its bearing on the origin of oceanic and continental alkali basalt, *Earth Planet. Sci. Lett.*, *72*, 23–38, 1985.

Graham, D. W., J. Lupton, F. Albarède, and M. Condomines, Extreme temporal homogeneity of helium isotopes at Piton de la Fournaise, Réunion Island, *Nature*, *347*, 545–548, 1990.

Graham, D. W., S. E. Humphris, W. J. Jenkins, and M. D. Kurz, Helium isotope geochemistry of some volcanic rocks from St. Helena, *Earth Planet. Sci. Lett.*, *110*, 121–131, 1992.

Graham, D. W., D. M. Christie, K. S. Harpp, and J. E. Lupton, Mantle plume helium in submarine basalts from the Galápagos platform, *Science*, *262*, 2023–2026, 1993.

Halliday, A. N., A. P. Dickin, A. E. Fallick, and J. G. Fitton, Mantle dynamics: A Nd, Sr, Pb and O isotopic study of the Cameroon Line Volcanic Chain, *J Petrol.*, *29*, 181–211, 1988.

Halliday, A. N., J. P. Davidson, P. Holden, C. DeWolf, D.-C. Lee, and J. G. Fitton, Trace-element fractionation in plumes and the origin of HIMU mantle beneath the Cameroon line, *Nature*, *347*, 523–528, 1990.

Halliday, A. N., D.-C. Lee, S. Tommasini, G. R. Davies, C. Paslick, J. G. Fitton, and D. E. James, Incompatible trace elements in OIB and MORB and source enrichment in the sub-oceanic mantle, *Earth Planet. Sci. Lett.*, *133*, 379–395, 1995.

Hanyu, T., and I. Kaneoka, The uniform and low $^3He/^4He$ ratios of HIMU basalts as evidence for their origin as recycled materials, *Nature*, *390*, 273–276, 1997.

Hanyu, T., and I. Kaneoka, Open system behavior of helium in case of the Himu source, *Geophys. Res. Lett.*, *25*(5), 687–690, 1998.

Hart, S. R., A large-scale isotope anomaly in the Southern Hemsiphere mantle, *Nature*, *309*, 753–757, 1984a.

Hart, S. R., He diffusion in olivine, *Earth Planet. Sci. Lett.*, *70*, 297–302, 1984b.

Hart, S. R., and H. Staudigel, Isotopic characterization and identification of recycled components, in *Crust/Mantle Recycling at Convergence Zones*, edited by S. R. Hart and L. Gülen, pp. 15–28, Kluwer Acad., Norwell, Mass., 1989.

Hart, S. R., and A. Zindler, Constraints on the nature and development of chemical heterogeneities in the mantle, in *Mantle Convection*, edited by W. R. Peltier, pp. 261–387, Gordon and Breach, Newark, N. J., 1989.

Hart, S. R., D. C. Gerlach, and W. M. White, A possible new Sr-Nd-Pb mantle array and consequences for mantle mixing, *Geochim. Cosmochim. Acta*, *50*, 1551–1557, 1986.

Hilton, D. R., J. Barling, and G. E. Wheller, Effect of shallow-level contamination on the helium isotope systematics of ocean-island lavas, *Nature*, *373*, 330–333, 1995.

Hiyagon, H., and M. Ozima, Partition of gases between olivine and basalt melt, *Geochim. Cosmochim. Acta*, *50*, 2045–2057, 1986.

Hiyagon, H., M. Ozima, B. Marty, S. Zashu, and H. Sakai, Noble gases in submarine glasses from mid-oceanic ridges and Loihi seamount: Constraints on early history of the Earth, *Geochim. Cosmochim. Acta*, *56*, 427–437, 1992.

Hofmann, A. W., Mantle geochemistry: The message from oceanic volcanism, *Nature*, *385*, 219–229, 1997.

Hofmann, A. W., and W. M. White, Mantle plumes from ancient ocean crust, *Earth Planet. Sci. Lett.*, *57*, 421–436, 1982.

Hohenberg, C. M., High sensitivity pulse counting mass spectrometer system for noble gas analyses, *Rev. Sci. Instrum.*, *58*(8), 1075–1082, 1980.

Honda, M., and I. McDougall, Primordial helium and neon in the Earth: A speculation on early degassing, paper presented at Seventh Annual V. M. Goldschmidt Conference, Lunar and Planet. Inst., Tucson, Ariz., 1997.

Honda, M., I. McDougal, D. Patterson, A. Doulgeris, and D. Clague, Noble gases in submarine pillow basalts from Loihi and Kilauea, Hawaii: A solar component in the Earth, *Geochim. Cosmochim. Acta*, *57*, 859–874, 1993a.

Honda, M., I. McDougall, and D. Patterson, Solar noble gases in the Earth: Systematics of helium-neon isotopes in mantle derived samples, *Lithos*, *30*, 257–265, 1993b.

Irving, A. J., Petrology and geochemistry of composite ultramafic xenoliths in alkalic basalts and implications for magmatic processes within the mantle, *Am. J. Sci.*, *280A*, 389–426, 1980.

Jochum, K. P., A. W. Hofmann, E. Ito, H. M. Seufert, and W. M. White, K, U and Th in mid-ocean ridge basalt glasses and heat production, K/U and K/Rb in the mantle, *Nature*, *306*, 431–436, 1983.

Kaneoka, I., N. Takaoka, and D. A. Clague, Noble gas systematics for coexisting glass and olivine crystals in basalts and dunite xenoliths from Loihi Seamount, *Earth Planet. Sci. Lett.*, *66*, 427–437, 1983.

Kaneoka, I., N. Takaoka, and B. G. J. Upton, Noble gas systematics in basalts and a dunite nodule from Réunion and Grand Comore Islands, Indian Ocean, *Chem. Geol.*, *59*, 35–42, 1986.

Kellogg, L. H., and G. J. Wasserburg, The role of plumes in mantle helium fluxes, *Earth Planet. Sci. Lett.*, *99*, 276–289, 1990.

Kennedy, B. M., J. H. Reynolds, S. P. Smith, and A. H. Truesdell, Helium isotopes: Lower geyser basin, Yellowstone National Park, *J. Geophys. Res.*, *92*(B12), 12,477–12,489, 1987.

Kurz, M. D., In situ production of terrestrial cosmogenic helium and some applications to geochronology, *Geochim. Cosmochim. Acta*, *50*, 2855–2862, 1986.

Kurz, M. D., and D. P. Kammer, Isotopic evolution of Mauna Loa Volcano, *Earth Planet. Sci. Lett.*, *103*, 257–269, 1991.

Kurz, M. D., W. J. Jenkins, and S. R. Hart, Helium isotopic systematics of oceanic islands and mantle heterogeneity, *Nature*, *297*, 43–46, 1982.

Kurz, M. D., W. J. Jenkins, S. R. Hart, and D. Clague, Helium isotopic variations in volcanic rocks from Loihi Seamount and the island of Hawaii, *Earth Planet. Sci. Lett.*, *66*, 388–406, 1983.

Kurz, M. D., P. S. Meyer, and H. Sigurdsson, Helium isotopic systematics within the neovolcanic zones of Iceland, *Earth Planet. Sci. Lett.*, *74*, 291–305, 1985.

Kurz, M. D., J. J. Gurney, W. J. Jenkins, and D. E. Lott III, Helium isotope variability within single diamonds from the Orapa kimberlite pipe, *Earth Planet. Sci. Lett.*, *86*, 57–68, 1987.

Kurz, M. D., T. C. Kenna, J. C. Lassiter, and D. J. DePaolo, Helium isotopic evolution of Mauna Kea Volcano: First results from the 1-km drill core, *J. Geophys. Res.*, *101*(B5), 11,781–11,791, 1996.

Kyser, T. K., and W. Rison, Systematics of rare gas isotopes in basic lavas and ultramafic xenoliths, *J. Geophys. Res.*, *87*(B7), 5611–5630, 1982.

Lee, D.-C., A. N. Halliday, J. G. Fitton, and G. Poli, Isotopic variation with distance and time in the oceanic sector of the Cameroon line: Evidence for a mantle plume origin and rejuvination of magma transport paths, *Earth Planet. Sci. Lett.*, *123*, 119–138, 1994.

Lee, D.-C., A. N. Halliday, G. R. Davies, E. J. Essene, J. G. Fitton, and R. Temdjim, Melt enrichment of shallow depleted mantle: a detailed petological, trace element and isotopic study of mantle derived xenoliths and megacrysts from the Cameroon line, *J. Petrol.*, *37*, 415–441, 1996.

Marty, B., and A. Jambon, C/^{3}He in volatile fluxes from the solid Earth: Implications for carbon geodynamics, *Earth Planet. Sci. Lett.*, *83*, 16–26, 1987.

Marty, B., I. Appora, J. A. Barrat, C. Deniel, P. Vellutini, and P. Vidal, He, Ar, Sr, Nd, and Pb isotopes in volcanic rocks from Afar: Evidence for a primitive mantle component and constraints on magmatic sources, *Geochem. J.*, *27*, 219–228, 1993a.

Marty, B., V. Meynier, E. Nicolini, E. Griesshaber, and J. P. Toutain, Geochemistry of gas emanations: a case study of the Réunion Hot Spot, Indian Ocean, *Appl. Geochem.*, *8*, 141–152, 1993b.

Marty, B., R. Pik, and Y. Gezahegn, Helium isotopic variations in Ethiopian plume lavas: Nature of magmatic sources and limit on lower mantle contribution, *Earth Planet. Sci Lett.*, *144*, 223–237, 1996.

Mercier, J.-C. C., and A. Nicolas, Textures and fabrics of upper-mantle peridotites as illustrated by xenoliths from basalts, *J. Petrol.*, *16*(2), 454–487, 1975.

Moreira, M., J. Kunz, and C. J. Allègre, Rare gas systematics in popping rock: Isotopic and elemental compositions in the upper mantle, *Nature*, *279*, 1178–1181, 1998.

Nakamura, Y., and M. Tatsumoto, Pb, Nd, and Sr isotopic evidence for a multicomponent source for rocks of the Cook-Austral Islands and heterogeneities of mantle plumes, *Geochim. Cosmochim. Acta*, *52*, 2909–2924, 1988.

Niedermann, S., W. Bach, and J. Erzinger, Noble gas evidence for a lower mantle component in MORBs from the southern East Pacific Rise: Decoupling of helium and neon isotope systematics, *Geochim. Cosmochim. Acta*, *61*, 2697–2715, 1997.

O'Nions, R. K., and I. N. Tolstikhin, Behaviour and residence times of lithophile and rare gas tracers in the upper mantle, *Earth Planet. Sci. Lett.*, *124*, 131–138, 1994.

Ozima, M., and F. A. Podosek, *Noble Gas Geochemistry*, Cambridge Univ. Press, New York, 1983.

Pasteris, J. D., Fluid inclusions in mantle xenoliths, in *Mantle Xenoliths*, edited by P. H. Nixon, pp. 691–707, John Wiley, New York, 1987.

Porcelli, D., and G. J. Wasserburg, Mass transfer of helium, neon, argon, and xenon through a steady-state upper mantle, *Geochim. Cosmochim. Acta*, *59*, 4921–4937, 1995.

Poreda, R. J., and K. A. Farley, Rare gases in Samoan xenoliths, *Earth Planet. Sci. Lett.*, *113*, 129–144, 1992.

Poreda, R., J. G. Schilling, and H. Craig, Helium and hydrogen isotopes in ocean-ridge basalts north and south of Iceland, *Earth Planet. Sci. Lett.*, *78*, 1–17, 1986.

Ringwood, A. E., *Compositions and Petrology of the Earth's Mantle*, McGraw-Hill, New York, 1975.

Ringwood, A. E., Slab-mantle interactions, 3, Petrogenesis of intraplate magmas and structure of the upper mantle, *Chem. Geol.*, *82*, 187–207, 1990.

Rison, W., and H. Craig, Helium isotopes and mantle volatiles in Loihi Seamount and Hawaiian Island basalts and xenoliths, *Earth Planet. Sci. Lett.*, *66*, 407–426, 1993.

Roden, M. F., T. Trull, S. R. Hart, and F. A. Frey, New He, Nd, Pb, and Sr isotopic constraints on the constitution of the Hawaiian plume: Results from Koolau Volcano, Oahu, Hawaii, USA, *Geochim. Cosmochim. Acta*, *58*, 1431–1440, 1994.

Roedder, E., *Fluid Inclusions*, Mineral. Soc. of Am., Washington, D. C., 1984.

Roselieb, K., H. Büttner, U. Eicke, U. Köhler, and M. Rosenhauer, Pressure dependence of Ar and Kr diffusion in a jadeite melt, *Chem. Geol.*, *128*, 207–216, 1996.

Sano, Y., M. Kusakabe, J. Hirabayashi, Y. Nojiri, H. Shinohara, T. Njine, and G. Tanyileke, Helium and carbon fluxes in lake Nyos, Cameroon: Constraints on next gas burst, *Earth Planet. Sci. Lett.*, *99*, 303–314, 1990.

Sarda, P., T. Staudacher, and C. J. Allègre, Neon isotopes in submarine basalts, *Earth Planet. Sci. Lett.*, *91*, 73–88, 1988.

Scarsi, P., and H. Craig, Helium isotope ratios in Ethiopian Rift basalts, *Earth Planet. Sci. Lett.*, *144*, 505–516, 1996.

Staudacher, T., and C. J. Allègre, Recycling of oceanic crust and sediments: The noble gas subduction barrier, *Earth Planet. Sci. Lett.*, *89*, 173–183, 1988.

Staudacher, T., M. D. Kurz, and C. J. Allègre, New noble-gas data on glass samples from Loihi seamount and Hualalai and on dunite samples from Loihi and Réunion island, *Chem. Geol.*, *56*, 193–205, 1986.

Sun, S.-S., and W. F. McDonough, Chemical and isotopic systematics of oceanic basalts: implications for mantle compositions and processes, in *Magmatism in Ocean Basins*, edited by A. D. Saunders and M. J. Norry, pp. 313–345, Blackwell Sci., Malden, Mass., 1989.

Taylor, R. N., M. F. Thirwall, B. J. Murton, D. R. Hilton, and M. A. M. Gee, Isotopic constraints on the influence of the Icelandic plume, *Earth Planet. Sci. Lett.*, *148*, E1–E8, 1997.

Trull, T. W., and M. D. Kurz, Experimental measurements of ^{3}He and ^{4}He mobility in olivine and clinopyroxene at magmatic temperatures, *Geochim. Cosmochim. Acta*, *57*, 1313–1324, 1993.

Trull, T. W., M. D. Kurz, and W. J. Jenkins, Diffusion of cosmogenic ^{3}He in olivine and quartz: Implications for surface exposure dating, *Earth Planet. Sci. Lett.*, *103*, 241–256, 1991.

Trull, T., S. Nadeau, F. Pineau, M. Polve, and M. Javoy, C-He system-

atics in hotspot xenoliths: Implications for mantle carbon contents and carbon recycling, *Earth Planet. Sci. Lett.*, *118*, 43–64, 1993.

Valbracht, P. J., H. Staudigel, M. Honda, I. McDougall, and G. R. Davies, Isotopic tracing of volcanic source regions from Hawaii: Decoupling of gaseous from lithophile magma components, *Earth Planet. Sci. Lett.*, *144*, 185–198, 1996.

Vidal, P., C. Chauvel, and R. Brousse, Large mantle heterogeneity beneath French Polynesia, *Nature*, *307*, 536–538, 1984.

Watson, E. B., Calcium diffusion in a simple silicate melt to 30 kbar, *Geochim. Cosmochim. Acta*, *43*, 313–322, 1979.

Watson, E. B., Diffusion in magmas at depth in the Earth: The effects of pressure and dissolved H_2O, *Earth Planet. Sci. Lett.*, *52*, 291–301, 1981.

Weaver, B. L., The origin of ocean island basalt end-member compositions: Trace element and isotopic constraints, *Earth Planet. Sci. Lett.*, *104*, 381–397, 1991.

White, W. M., $^{238}U/^{204}Pb$ in MORB and open system evolution of the depleted mantle, *Earth Planet. Sci. Lett.*, *115*, 211–226, 1993.

White, W. M., and A. W. Hofmann, Sr and Nd isotope geochemistry of oceanic basalts and mantle evolution, *Nature*, *296*, 821–825, 1982.

Yatsevich, I., and M. Honda, Production of nucleogenic neon in the Earth from natural radioactive decay, *J. Geophys. Res.*, *102*(B5), 10,291–10,298, 1997.

Zhang, Y., and Z. Xu, Atomic radii of noble gas elements in condensed phases, *Am. Mineral.*, *80*, 670–675, 1995.

Zindler, A., and S. R. Hart, Chemical geodynamics, *Annu. Rev. Earth Planet. Sci.*, *14*, 493–571, 1986.

C. J. Ballentine, Institute for Isotope Geology and Mineral Resources, Department of Earth Sciences, ETH Zürich N0 C61, Sonneggstrasse 5, CH-8092, Zürich, Switzerland. (ballentine@erdw.ethz.ch)

D. N. Barfod, Isotope Geosciences Unit, Scottish Universities Research and Reactor Center, East Kilbride G75 0QF, Scotland, U.K.

J. G. Fitton, Grant Institute of Geology, University of Edinburgh, West Mains Road, Edinburgh EH9 3JW, Scotland, U.K. (gfitton@glg.ed.ac.uk)

A. N. Halliday, Institute for Isotope Geology and Mineral Resources, Department of Earth Sciences, ETH Zürich N0 C61, Sonneggstrasse 5, CH-8092, Zürich, Switzerland. (halliday@erdw.ethz.ch)

(Received December 3, 1998; revised July 13, 1999;
accepted August 10, 1999.)